

**THERMAL DIFFUSIVITY IN Eu^{3+}
DOPED GLASSES**

By

RICARDO NIEVES

Bachelor of Science

State University of New York College at Cortland

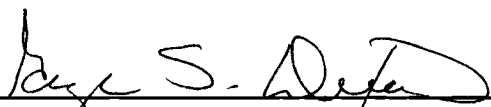
Cortland, NY

1991

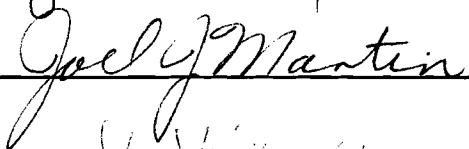
Submitted to the Faculty of the
Graduate College of the
Oklahoma State University
in partial fulfillment of
the requirements for
the Degree of
MASTER OF SCIENCE
December, 1995

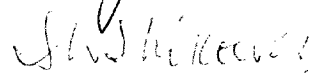
**THERMAL DIFFUSIVITY IN Eu^{3+}
DOPED GLASSES**

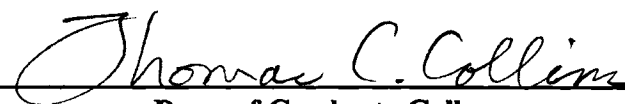
Thesis Approved:



Thesis Advisor







Dean of Graduate College

ACKNOWLEDGMENTS

I wish to thank my advisor and committee chairman, Dr. George S. Dixon, for his valuable assistance and encouragement throughout my educational experience here at Oklahoma State University. Especially, for taking the time to discuss with me those areas in my research that I had questions about and could not quite understand at the time. Thanks to my committee members, Dr. Joel J. Martin and Dr. Stephen W.S. McKeever, for taking time out from their busy schedules to serve on my committee.

Thanks to Susan Cantrell and Cheryl Outon in the Physics Dept. Office, for their assistance throughout my years here. Thanks to Patricia Watson for conducting the Raman experiments on my samples. Thanks to Rolando Diaz from the Multicultural Development and Assessment Center, for his encouragement and support as a friend.

Most important, I wish to thank my wife Leslie Carol Mayes Nieves. Had I not meet and married Leslie, I probably would not have remained at Oklahoma State University and completed my thesis. I wish to thank her for her support and encouragement throughout our years together. During the times when I felt like I would never finish this thesis she had maintained her faith in me and pushed me forward. It is to her to whom I dedicate this thesis to with all my love and affection.

LESLIE, I LOVE YOU

TABLE OF CONTENTS

	Page
I. INTRODUCTION.....	1
• Amorphous Solids.....	2
• Structure of Glasses.....	7
• Continuous Random Network.....	13
• Modified Random Network.....	14
• Phonons in Glasses.....	17
• Statement of Purpose.....	22
II. EXPERIMENTAL PROCEDURE.....	23
• Samples.....	23
• Experimental Setup.....	23
• Procedure.....	26
III. RESULTS and DISCUSSION.....	32
IV. CONCLUSION.....	54
REFERENCES.....	55

LIST OF TABLES

Table	Page
1. Sample Compositions.....	24
2. Physical Properties of the Glasses.....	41

LIST OF FIGURES

Figure	Page
1	The two general cooling paths by which a liquid can condense into the solid state. Route 1 is the path to the crystalline state; route 2 is the path to the amorphous state.....3
2	Volume-versus-temperature cooling curves for an organic material in the neighborhood of the glass transition. $V(T)$ is shown for two greatly different cooling rates. In addition, the coefficient of thermal expansion $\alpha(T)$ for the fast-cooling curve (0.02hr) is also shown. The break in $V(T)$, and the corresponding step in $\alpha(T)$, signal the occurrence of the liquid-glass transition.....5
3	Specific heat capacity C_p -versus-temperature for a crystal and a glass. T_g marks the glass transition, and T_m signifies the melting temperature of the crystalline phase.....6
4	Schematic representation of short-range order in covalent glass systems defined in terms of intra-polyhedral and inter-polyhedral quantities.....9
5	Radial distribution function for crystalline and amorphous germanium.....11
6	The relative orientation of two corner sharing tetrahedra in a SiO_2 glass. In addition to the two dihedral angles δ and Δ , the SRO quantities r (nearest-neighbor distance) and ψ (intrapolyhedral angle which is the same as θ_{jij} in figure 4) are shown.....12
7	Left: Hypothetical representation of a crystalline compound A_2O_3 . Right: The Zachariasen model for the glassy form of the same A_2O_3 compound.....15
8	The Modified Random Network (MRN) model for the structure of glass. The dashed bonds represent ionic interaction. The regions that are not shaded represent the modifier channels.....16
9	The thermal conductivity as a function of temperature of crystalline quartz(I) and fused quartz(II).....18
10	Average phonon mean free path as a function of temperature for various glasses

	and SiO ₂ crystal.....	21
11	Molar mass of the samples vs. europium concentration.....	22
12	Schematic representation of the experimental setup.....	27
13	Typical temperature vs time data. The upper curve is for the thermocouple closest to the heater and the lower curve is for the thermocouple farthest away from the heater.....	29
14	Plot of $\partial T/\partial t$ vs $\partial^2 T/\partial x^2$ calculated from the data of figure 13. The slope of this curve is the thermal diffusivity, α	30
15	Thermal diffusivity as a function of temperature for the Bragg5 sample. In addition, the individual contributions to the thermal diffusivity of the extended and localized phonons is shown.....	33
16	Thermal diffusivity as a function of temperature for the Bragg6 sample.....	34
17	Thermal diffusivity as a function of temperature for the Bragg7 sample.....	35
18	Thermal diffusivity as a function of temperature for the Bragg8 sample.....	36
19	Thermal diffusivity as a function of temperature for the Bragg9 sample.....	37
20	Thermal diffusivity as a function of temperature for the Bragg10 sample.....	38
21	The thermal diffusivities as a function of temperature for all six samples. The caption in the upper right hand corner is the diffusivities in an expanded scale for clarity.....	39
22	Raman spectrum of the Bragg5 sample. The main figure shows the region of the mobility edge. The inset shows the full Raman spectrum for this sample.....	42
23	Raman spectrum of the Bragg6 sample. The main figure shows the region of the mobility edge. The inset shows the full Raman spectrum for this sample.....	43
24	Raman spectrum of the Bragg7 sample. The main figure shows the region	

	of the mobility edge. The inset shows the full Raman spectrum for this sample.....	44
25	Raman spectrum of the Bragg8 sample. The main figure shows the region of the mobility edge. The inset shows the full Raman spectrum for this sample.....	45
26	Raman spectrum of the Bragg9 sample. The main figure shows the region of the mobility edge. The inset shows the full Raman spectrum for this sample.....	46
27	Raman spectrum of the Bragg10 sample. The main figure shows the region of the mobility edge. The inset shows the full Raman spectrum for this sample.....	47
28	Schematic representation of the thermally activated hopping of localized phonon process.....	50

	of the mobility edge. The inset shows the full Raman spectrum for this sample.....	44
25	Raman spectrum of the Bragg8 sample. The main figure shows the region of the mobility edge. The inset shows the full Raman spectrum for this sample.....	45
26	Raman spectrum of the Bragg9 sample. The main figure shows the region of the mobility edge. The inset shows the full Raman spectrum for this sample.....	46
27	Raman spectrum of the Bragg10 sample. The main figure shows the region of the mobility edge. The inset shows the full Raman spectrum for this sample.....	47
28	Schematic representation of the thermally activated hopping of localized phonon process.....	50

CHAPTER I

INTRODUCTION

In the past few decades much intense research interest in amorphous solids has been driven by the technological importance of these materials[1]. Examples of the application of amorphous solids include optical fibers in telecommunications, solar cells, sensors, nuclear radiation containment, microelectronics, and as structural materials[1,2]. Furthermore, in certain applications where amorphous solids can be used in place of crystalline materials, it is better to do so, since these crystalline materials can be prohibitively expensive to fabricate[1]. The fact that one can control the viscosity of the melt of amorphous materials provides a valuable processing advantage in the preparation of products formed from glasses[1].

In this thesis, a study of the thermal diffusivity of a set of aluminosilicate glasses is presented. Specifically, the thermal diffusivity as a function of temperature for a set of six glasses with europium concentration ranging from 0 to 5 molar percent, was studied. The compositional formula of the set of glasses studied was $(0.70(\text{SiO}_2)0.03(\text{Al}_2\text{O}_3)0.12(\text{MgO})0.15(\text{Na}_2\text{O}))_{1-x}(\text{Eu}_2\text{O}_3)_x$. The data obtained in this experiment will be analyzed and shown to adhere to the two-carrier model for thermal transport in glasses introduced by Dixon and coworkers[3,4].

Before getting into the details of this experiment a brief description of the physics of amorphous solids, taken from the literature, is presented so that a general idea as to what materials fall under amorphous solids; what are some of their properties, and how do these properties contribute to both, the difficulty and ease of studying amorphous materials is obtained. In particular, the formation, structure, models, and modes of

vibration of amorphous solids are briefly covered.

Amorphous Solids

Amorphous materials can be defined as those materials which are topologically disordered and which do not exhibit periodicity characteristic of crystals, or the long-range orientational order characteristic of quasicrystals. Short of possessing the dynamic disorder characteristic of fluids, amorphous materials are among the most disordered of materials[5]. As figure 1 shows, a liquid may either solidify discontinuously into a crystalline solid or continuously into an amorphous solid. Almost all materials can be prepared as amorphous solids. One key to which path a liquid will follow in solidifying is speed; how fast the melt is cooled[1]. Crystallization takes time since crystalline centers must first form and then grow, at the expense of the liquid which may have different local order, by outward propagation of the crystal/liquid interface. Furthermore, the liquid-crystal transition is marked by a discontinuity at T_f (freezing point) in the volume vs. temperature curve which is due to the abrupt contraction of the volume of the crystalline solid. On the other hand, it is found that if the cooling rate of the melt is high enough, T_f is bypassed, and the liquid phase persists until a lower temperature T_g , called the glass transition temperature, is reached. When this occurs, there is no volume discontinuity. Instead, $V(T)$ bends over in a narrow temperature range to acquire the small slope characteristic of the low thermal expansion of a solid[1]. In this temperature range the viscosity of the melt increases rapidly, approaching that of a crystalline solid. During the time the liquid is cooled from T_f to T_g , it is prone to nucleation and growth of crystallites. It is therefore essential in the preparation of amorphous solids that the cooling must

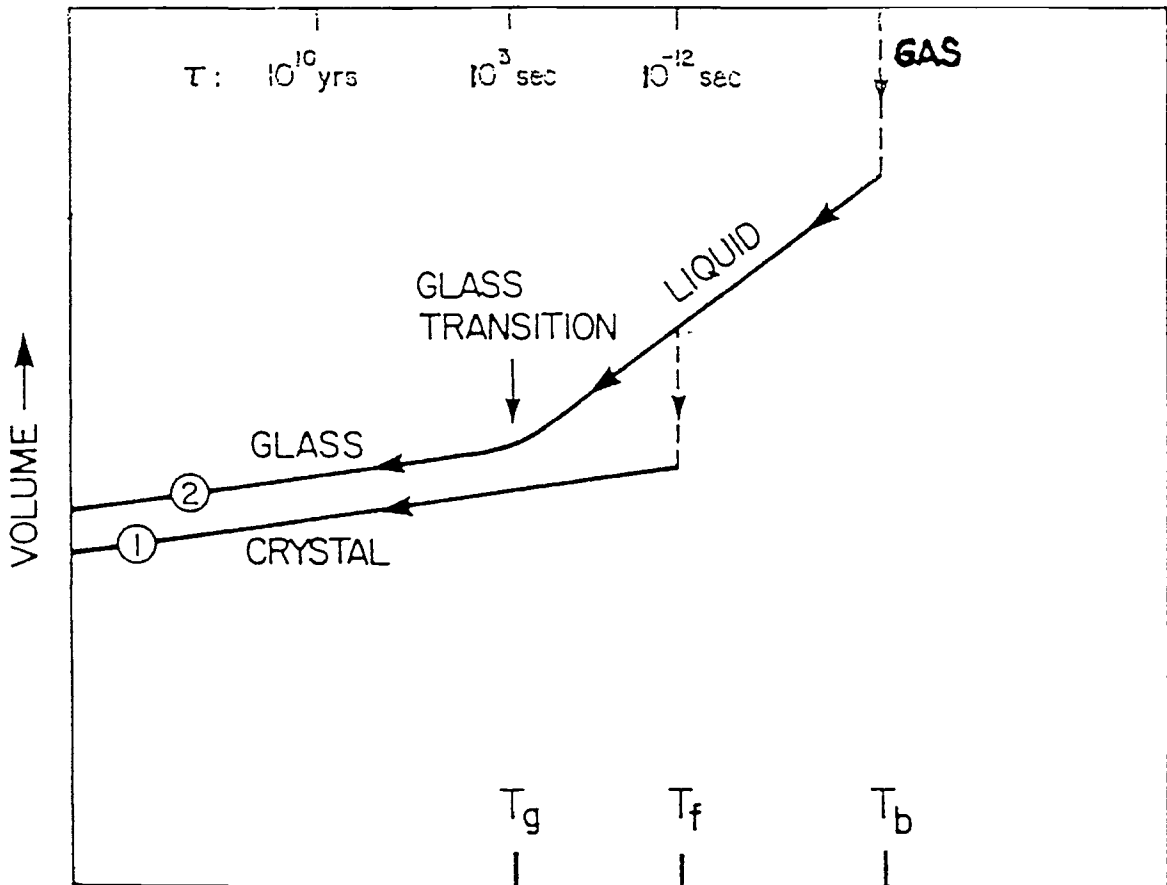


Figure 1. The two general cooling paths by which a liquid can condense into the solid state. Route 1 is the path to the crystalline state; route 2 is the path to the amorphous state (from ref. 1).

proceed “fast enough and far enough”; “far enough” in the sense that the quench must be taken to below the glass transition temperature ($T < T_g$), and “fast enough” in the sense that $T_g < T < T_f$ must be crossed in a time too short for crystallization to occur[1]. Typical cooling rates for glasses in the category of SiO_2 , As_2S_3 , and polystyrene are in the range from 10^{-4} to 10^{-10} K/sec[1].

As seen in figure 2, the glass transition temperature T_g depends on the cooling rate. The slower the cooling rate is the lower the temperature T_g at which the liquid solidifies to an amorphous solid. This is due to the temperature dependence of the molecular relaxation time τ [1]. The quantity $1/\tau$ characterizes the rate at which the atomic-scale structure of the system adapts itself to a change in temperature. The molecular relaxation time may increase from the order of 10^{-12} seconds at T_f to 10^{10} years in the interval between T_g and 50 K[1]. As T transverses the region near T_g , $\tau(T)$ becomes comparable to the time scale of the experiment. As T is lowered below T_g , τ becomes very large causing the material to lose its ability to rearrange its atomic configuration. The atoms essentially get frozen and remain in their positions indefinitely in a metastable state, where the only motion present is that of oscillation about their frozen equilibrium positions[1,5].

In addition to the different paths that amorphous and crystalline materials take in solidifying into a solid, one can further distinguish the solidification which occurs at T_g from that which occurs via crystallization at T_f by examining the response of either $C_p(T)$, the specific heat at constant pressure, or $\alpha(T)$, the thermal expansion coefficient, to a temperature-induced change of phase[1]. As illustrated in figures 2 and 3, the behavior of $C_p(T)$ and $\alpha(T)$ near T_g are qualitatively the same; Both the specific heat and the thermal

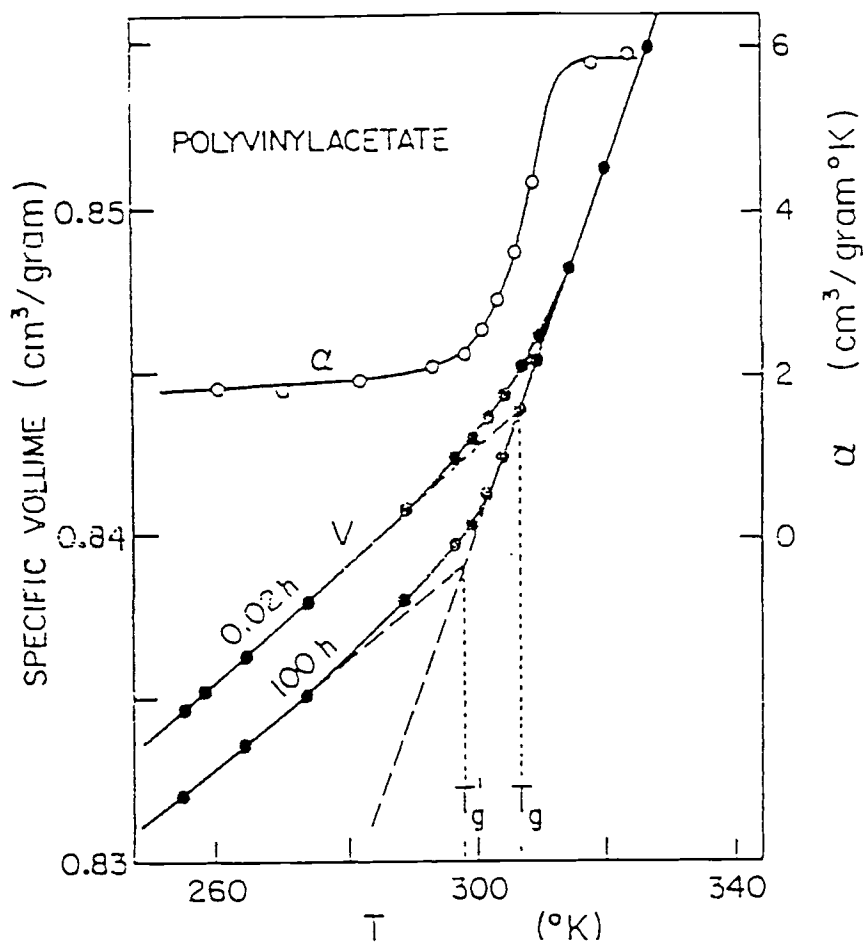


Figure 2. Volume-versus-temperature cooling curves for an organic material in the neighborhood of the glass transition. $V(T)$ is shown for two greatly different cooling rates. In addition, the coefficient of thermal expansion $\alpha(T)$ for the fast-cooling curve (0.02hr) is also shown. The break in $V(T)$, and the corresponding step in $\alpha(T)$, signal the occurrence of the liquid-glass transition (from ref. 1).

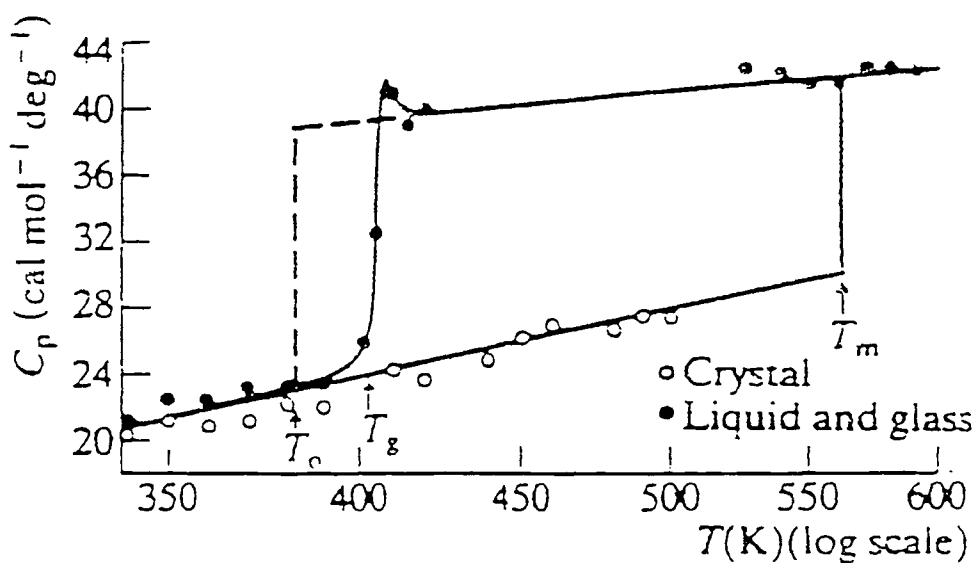


Figure 3. Specific heat capacity C_p -versus-temperature for a crystal and a glass. T_g marks the glass transition, and T_m signifies the melting temperature of the crystalline phase (from ref. 5).

expansion coefficient step up, in a narrow temperature interval, from a low value characteristic of the glass to a high value characteristic of the liquid[1]. While it has been argued that this behavior resembles a second-order transition[1], this may not be the case since the amorphous state is not a thermodynamic equilibrium state. Furthermore, true second-order transitions are characterized by a sharp change occurring at a single sharply definable temperature. While the step in $C_p(T)$ and $\alpha(T)$ are steep, they are not vertical discontinuities. The purpose of mentioning this is not to argue whether the behavior of $C_p(T)$ and $\alpha(T)$ are or are not second-order transitions, it is merely to emphasize the fact that, in terms of thermodynamic measurements, the glass transition is well defined[1]. To sum up, we can therefore say that the glass transition is marked(as a function of temperature) either by a change in slope of extensive thermodynamic quantities such as volume and entropy or, equivalently, as a “discontinuity” in derivative quantities such as specific heat or thermal expansivity[5].

Structure of Glasses

As was already mentioned in the previous section, the structure of glasses is characterized by topological disorder, so there is no long-range order(periodicity) in their structure. This makes studying the structure of glasses much more complicated than in their crystalline counterparts where an underlying periodic lattice exists from which one can describe the whole crystalline solid on the basis of a few atoms. However, this does not mean that glasses are structurally completely random at all length scales. In fact, covalent materials, in particular, exhibit a high degree of structural order at length scales corresponding to several atomic separations[5]. In other words, there is a high degree of

short-range order similar to that found in crystals. This is a consequence of the chemical bonding responsible for holding the solid together[1,5]. The importance of short-range order in glasses can be seen in those applications where a crystalline solid can be replaced by its glass counterpart. This is due to the fact that glassy materials often share the same coordination numbers and nearest-neighbor separation as their crystalline counterparts[5].

We can describe the atomic structure of glasses in terms of increasing length scales, distinguishing between short-range order(SRO) and medium-range order(MRO). Short-range order encompasses a length scale from 2 to 3Å and is associated with the nearest-neighbor environment of atoms. For the case of covalently-bonded glasses, the simplest description of SRO is in terms of local coordination polyhedra and their interconnectivity[5]. Thus, SRO can be characterized in terms of intra-polyhedral factors, such as the 2-body correlation quantities: r , the nearest-neighbor bond length, and z , the coordination number, which gives for a particular atom, the number of nearest neighbor atoms which surround that atom in the solid. In addition, the 3-body correlation quantities θ_{jij} , the intra-polyhedral bond angle between two atoms of type j connected through an atom of type i , N_u , the number of polyhedral units connected through each apex, and the inter-polyhedral angle θ_{jij} can be specified. These five quantities which are shown in figure 4, are sufficient to describe completely the SRO, both in terms of the type of coordination polyhedra present and the connectivity[5]. The coordination number z is the most valuable piece of structural information which provides evidence for a dominant role of covalent bonding($z \leq 4$) in the coupling of nearest-neighbor atoms[1]. By generalizing the idea of a single coordination number to a sequence of numbers embracing “shells” of neighbors at distances beyond the nearest ones, one is led to a more substantial structural

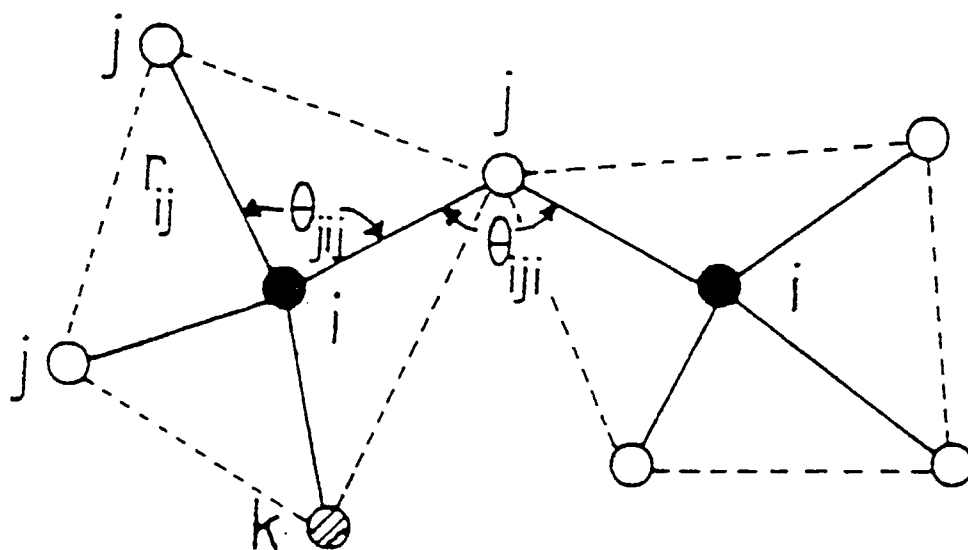


Figure 4. Schematic representation of short-range order in covalent glass systems defined in terms of intra-polyhedral and inter-polyhedral quantities (from ref. 5).

characterization called the radial distribution function (RDF)[1]. Direct evidence of the existence of SRO in glasses, in the form of well-defined nearest neighbor and next-nearest neighbor coordination shells, is provided by the presence of the clearly seen first and second peaks in the RDF in figure 5. However, the absence of long-range order manifests itself in the fact that, for glasses, discernible peaks in the RDF rarely occurs beyond third-nearest neighbors[1].

While the SRO of glasses is well known, the same cannot be said about medium-range order (also called intermediate range order). As it stands now, there is much controversy about what comprises the MRO of glasses since the terms used to describe MRO are not well defined[6]. This is due to the fact that while diffraction experiments tell us a wealth of information about SRO, they give us almost no information about MRO because of the absence of long-range order. As an example of the level of disagreement that exist in characterizing MRO, in ref. 6 the length scale of 3-5Å is considered as part of SRO for most materials, while in ref. 5 this range is considered as part of the local-scale MRO. Nevertheless, we can say a few things about what is generally accepted as representing MRO. In particular, the next successive length scale called in ref. 6 MRO, while in ref. 5, intermediate-scale MRO, extends from 5-10Å and specifies the dihedral angles δ and Δ ; the distribution of rings of completed bonds; and network connectivity[6]. The dihedral angles δ and Δ specify the relative orientation of adjacent tetrahedra as shown in figure 6. This type of MRO results in the formation of “superstructural units”[5]. While much more can be said about the classification and description of different length scales for the description of glass structure, we will stop here since this whole area in itself comprises a field of its own. The main objective of this section is to

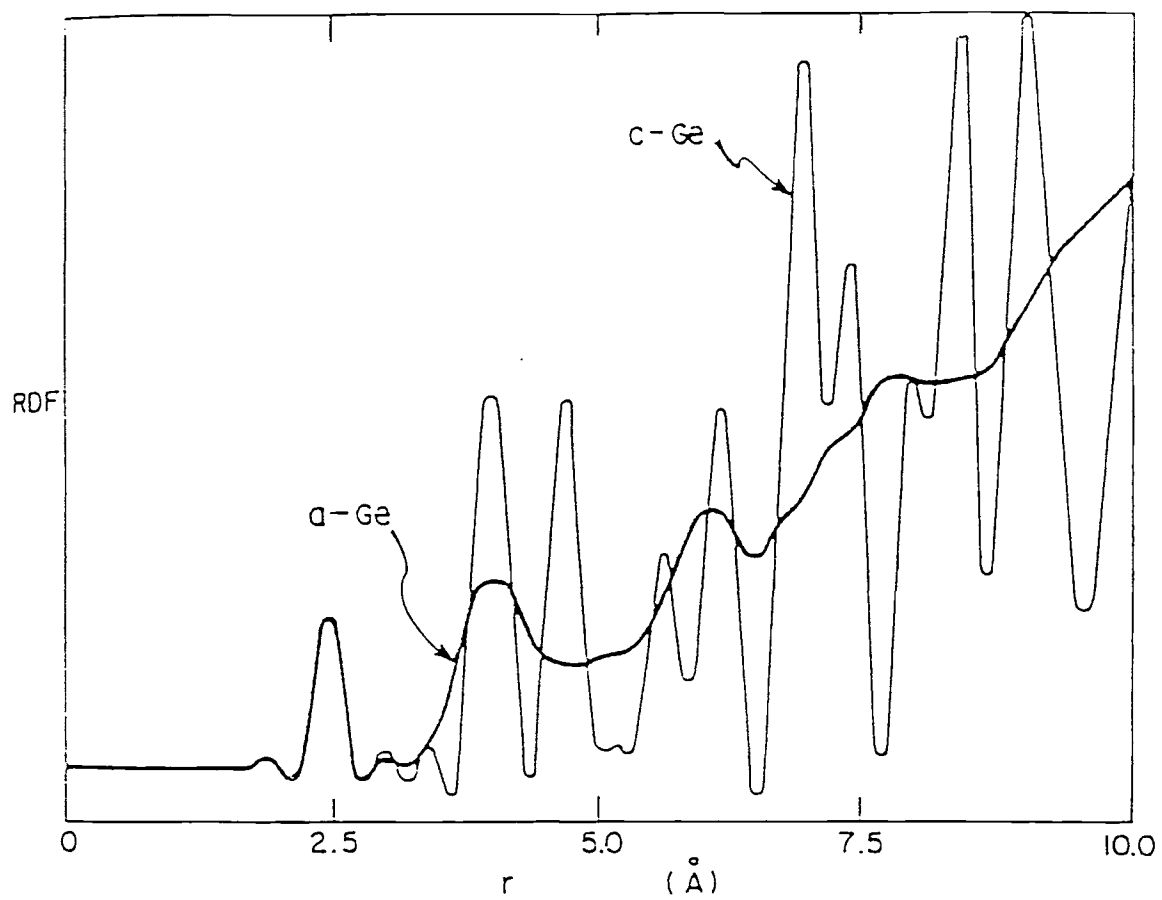


Figure 5. Radial Distribution function for crystalline and amorphous germanium (from ref. 1)

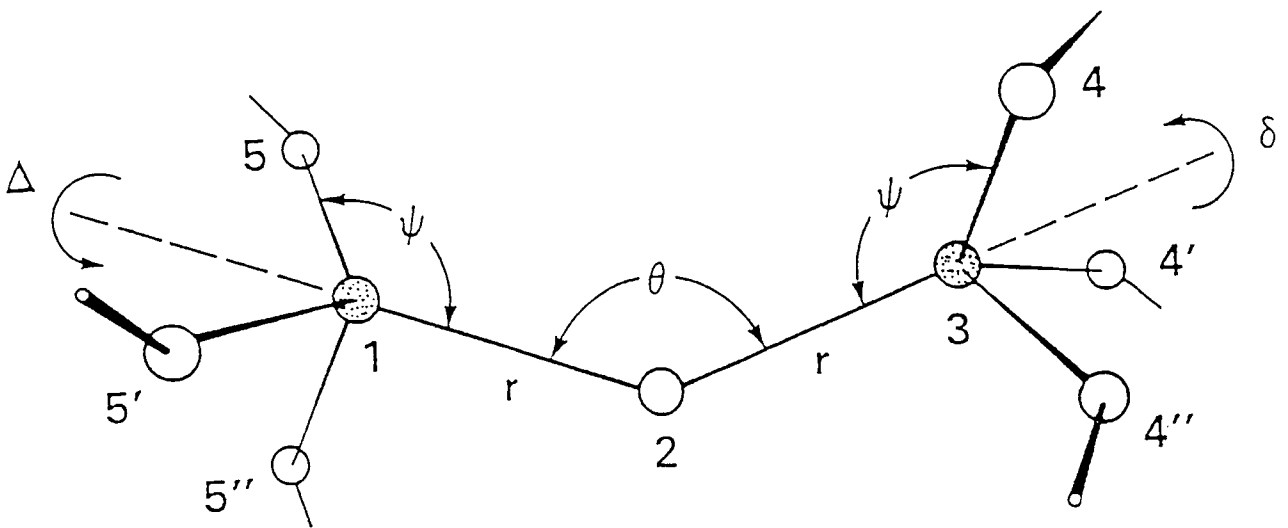


Figure 6. The relative orientation of two corner sharing tetrahedra in a SiO_2 glass. In addition to the two dihedral angles δ and Δ , the SRO quantities r (nearest-neighbor distance) and ψ (intrapolyhedral angle which is the same as θ_{jij} in figure 4) are shown (from ref. 6).

merely become familiar with the most important names and quantities used to describe glass structures.

Continuous Random Network

The Continuous Random Network (CRN) model was first proposed by Zachariasen[7] in 1932 to account for the structure of covalently bonded oxide glasses. Although this model represents an over idealization of the structure of the main classes of amorphous solids, it is nevertheless, the best available picture of the atomic-scale structure[1]. The CRN model is characterized by a large spread in bond angles θ (in figure 6). It is this spread in θ that is mainly responsible for the noncrystalline nature of the material[6]. The rules used in the building of SiO_2 networks are, that there only be Si-O bonds; Si be tetrahedrally bonded to four oxygens ($z=4$); each oxygen atom be bonded to two silicon atoms ($z=2$); constant bond lengths and O-Si-O bond angles (109°); a significant spread in Si-O-Si bond angles be permitted; the network be continuous (no dangling bonds); and tetrahedra share corners only (no edge or face-sharing)[1,6]. The first three rules assure that there be chemical ordering in the network, while the next two rules are based on the fact, that since Si is bonded to four oxygens, while oxygen is bonded to only two silicons, the bonds at the oxygens are much less constrained than those at the silicons and therefore are less costly in energy to deform[1,6]. Four years after Zachariasen came out with his model it was refined by Warren and coworkers[8] to allow the radius to be distributed over a narrow range centered about 1.61\AA and to include the assumption that the dihedral angle δ be randomly distributed, having no preferred value[6]. Zachariasen made no mention about dihedral angles and as a result lacked

specifications of MRO aside from the requirement that the tetrahedra share corners only[6]. In addition to these two modifications, the inter-polyhedral angle θ was interpreted from the RDF of x-ray diffraction experiments and was found to lie in the range of 120° to 180° with a mean value of 144° [6]. Figure 7 shows a schematic two-dimensional representation of the structure of a hypothetical crystalline compound with molecular formula A_2O_3 and the Zachariasen CRN model for the glassy form of the same compound.

Modified Random Network

Though glasses present certain complexities not found in crystals, there are certain advantages in studying them that would otherwise pose problems in crystals. For one, the compositional flexibility of glasses allows for the study of different types of additives over a wide range of concentrations without running into solubility limits. Furthermore, the structural changes created in the glasses by the additives enable one to study transport-structure correlations more readily than in crystalline solids[5]. This has sparked the development of a model based on the same principals as Zachariasen's CRN model called the Modified Random Network Model (MRN). In addition to glass forming cations and bridging oxygens which are characteristics of the CRN model, the MRN model also includes modifying cations and non-bridging oxygens with specific coordination spheres[5]. Modifying oxides like Na_2O and K_2O are seen as depolymerizing the glass former with the cations occupying holes and voids in the otherwise continuously connected random network[5]. In the MRN model, glass modifying oxides are believed to microsegregate from glass forming oxides at the atomic level as shown in figure 8. The

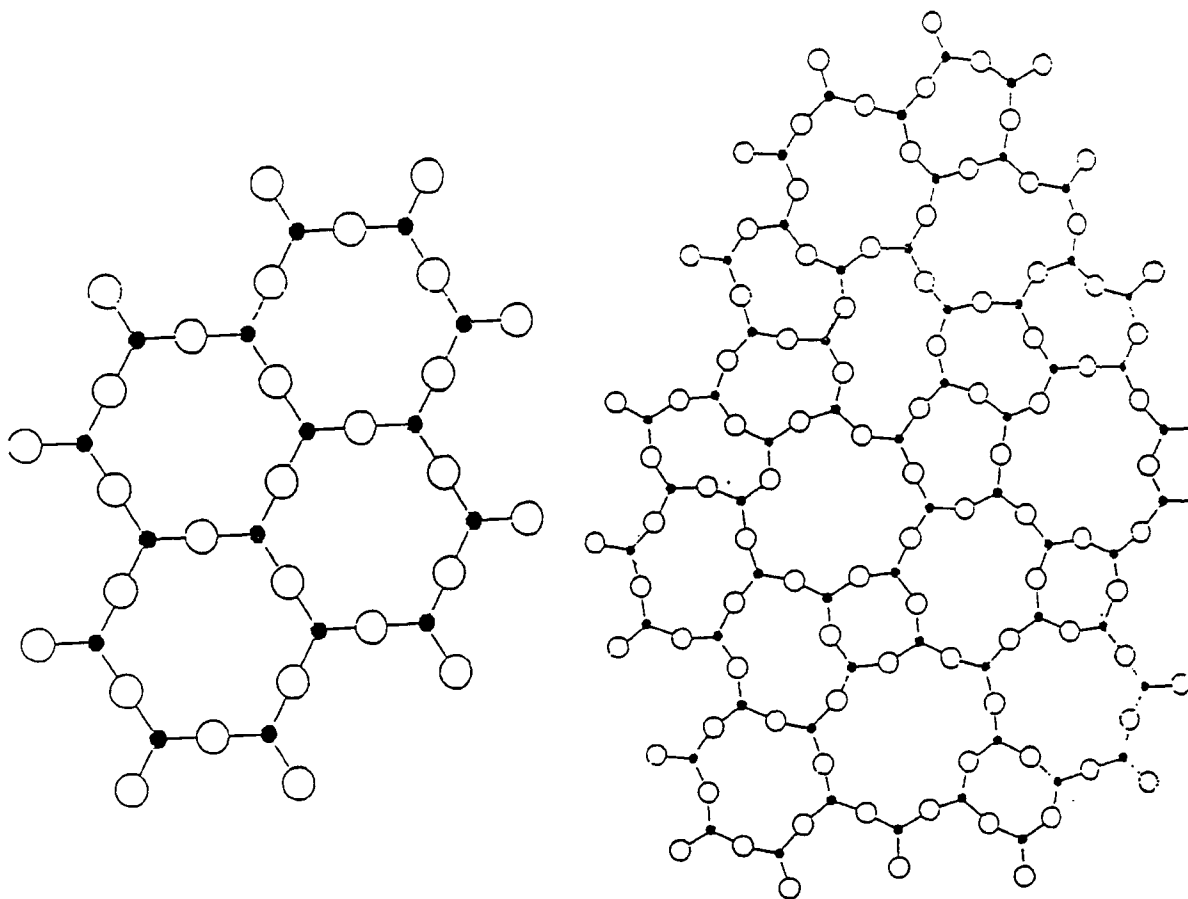


Figure 7. Left: Hypothetical representation of a crystalline compound A_2O_3 . Right: The Zachariasen model for the glassy form of the same A_2O_3 compound (from ref. 7).

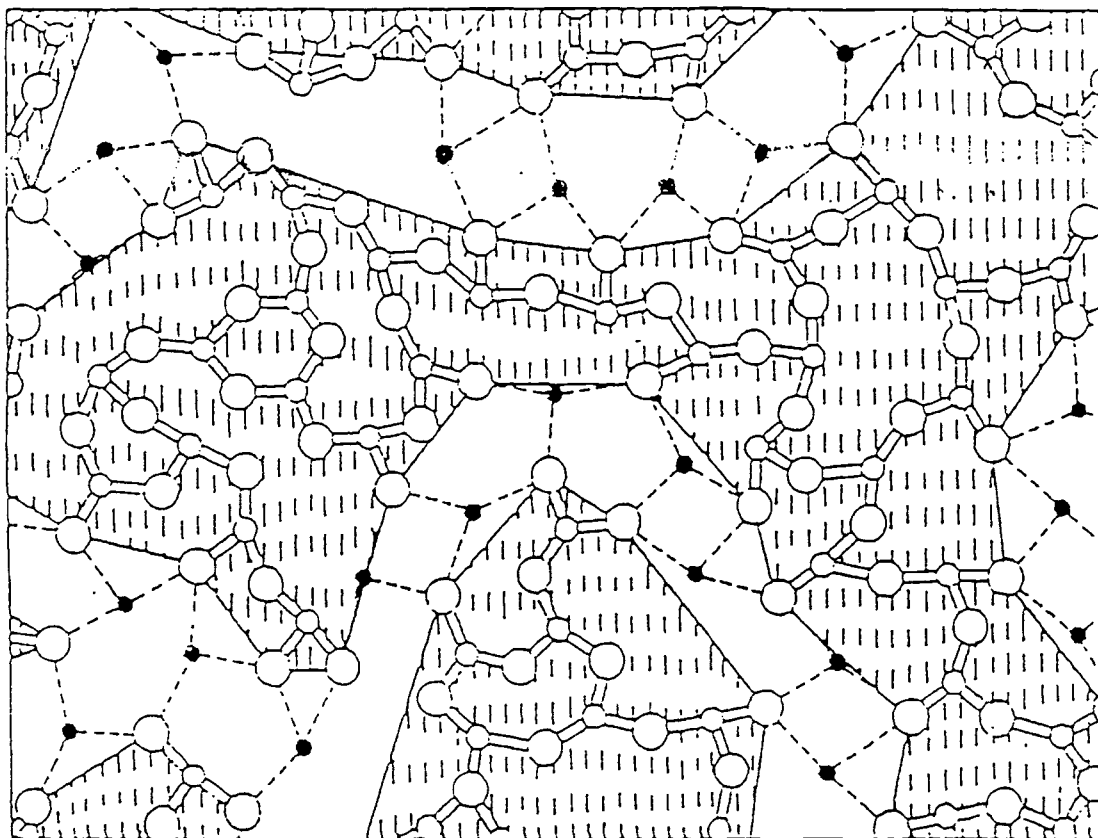


Figure 8. The Modified Random Network (MRN) model for the structure of glass. The dashed bonds represent ionic interaction. The regions that are not shaded represent the modifier channels (from ref. 5).

effect of modifiers are to simultaneously change the network structure and bonding which affects its rigidity, net charge, and distribution of interconnected interstices. These changes are reflected in the physical properties of the glass[5]. Network modifiers induce charges in the network by introducing ionic bonds between the positively-charged interstitial modifier cations and the now negatively-charged covalent chains. In silica glass for example, the alkali ions are incorporated into the network interstices, while excess oxygens are accommodated by the network by rupturing bridging oxygen bonds between adjacent Si-O tetrahedra and replacing them with non-bridging oxygen bonds[5].

Phonons in Glasses

The study of the thermal transport properties of amorphous solids has for the past two decades been focused around the behavior of the thermal conductivity and specific heat as a function of temperature, and the understanding and description of the processes which may or may not contribute to their behavior. While it has been well established[9-13] that phonons are responsible for the thermal diffusion in glasses, there is much disagreement as to how these phonons interact with each other and with other intrinsic properties of the material to give the observed behavior in the thermal conductivity[13]. While numerous models have been put forth ever since Zeller and Pohl[14] first presented experimental evidence that the thermal properties of amorphous solids differ remarkably from their crystalline counterparts at low temperature, only those models which are generally accepted as representing the behavior of the thermal conductivity in their respective temperature range will be briefly mentioned.

To begin, figure 9 displays the thermal conductivity as a function of temperature of

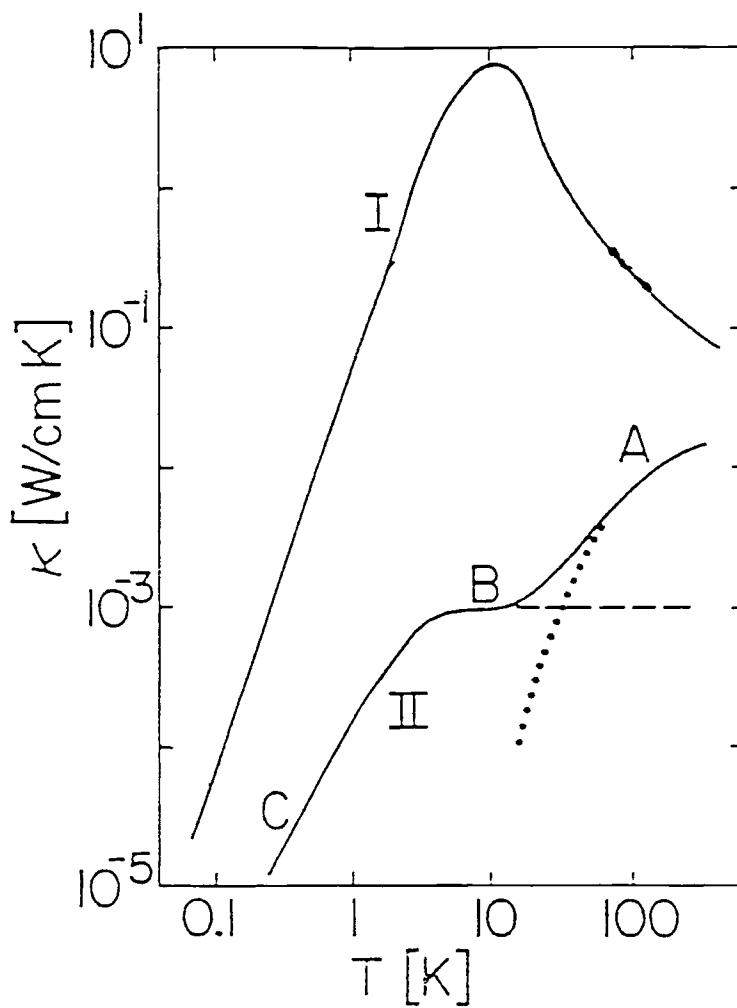


Figure 9. The thermal conductivity as a function of temperature of crystalline quartz(I) and fused quartz(II) (from ref. 13).

crystalline quartz(I) and fused quartz(II). It is easily seen that the behavior of these two materials are vastly different. In particular, the thermal conductivity of the amorphous solid is several orders of magnitude smaller than its crystalline counterpart[14]. Furthermore, it has been found that for a large variety of amorphous solids the thermal conductivities are very similar in form to that shown in figure 9 and differ in magnitude within a factor of 10[13,15]. In contrast, the thermal conductivity in crystalline solids can vary by as much as five orders of magnitude, with correspondingly different temperature dependencies[15]. The thermal conductivity curve for amorphous materials can be broken up into three distinct regions, A, B, and C, which are easily discernible in figure 9. While the scope of our experiment extends well into region A, the processes believed to be responsible for the behavior of the thermal conductivity in regions B and C will be briefly mentioned.

For temperatures less than 5 K, corresponding to region C, it has been shown by Zeller and Pohl[14] that the thermal conductivity varies as T^2 which is interpreted as a mean free path for phonons going as ω^{-1} . This T^2 behavior was first explained successfully through a model put forth by Anderson and coworkers[11] where low frequency extended phonons, similar to Debye phonons of crystalline solids, are scattered off localized two-level systems[9,13].

Proceeding on to higher temperatures, we encounter region B (the plateau where $\sim 5K < T < \sim 20K$, depending on the material) where the thermal conductivity is independent of temperature. This plateau region is believed to signal the onset of phonon localization[9-12]. In particular, it is believed that a mobility edge[9] or crossover frequency, ω_c , [11,12] exists where phonons with $\omega < \omega_c$ are extended states and those with

$\omega > \omega_c$ are localized. In the vicinity of the plateau the localized phonon population is spatially distributed throughout the material and therefore does not contribute to the thermal conductivity. On the other hand, the already excited extended phonons are in the Dulong-Petit region and so their contribution to the thermal conductivity is constant. This coupled with a constant sound velocity and mean free path for the phonons with frequencies less than ω_c results in the plateau[9,12]. Evidence of phonon localization is seen by the behavior of the phonon mean free path as a function of phonon frequency in figure 10, where it is shown that the mean free path of the phonons (assuming all are extended states) decreases dramatically in the vicinity of the plateau to a few atomic spacing. To date, it is still unclear as to why the phonon mean free path becomes so strongly frequency dependent (from a dependence of ω^{-1} at the lowest temperature region to an ω^{-x} dependence in the vicinity of the plateau, where $x \sim 4$). Jagannathan and coworkers[12] have attributed it to Rayleigh-like scattering and anharmonic coupling between the extended state phonons and localized states. Further support of the localization of phonons is mentioned in references [10] and [12], where the mobility edge or crossover frequency is seen to occur approximately where the Ioffe-Regel condition is satisfied, which is generally accepted as signaling vibrational localization[10,12].

Moving on to region A, we see that, as the temperature increases above the plateau, the thermal conductivity increases approximately linearly. This behavior is attributed to phonon assisted hopping of the localized vibrational modes[9,10] or phonon-induced fracton-hopping[11,12]. In particular, as the temperature for frequencies $\omega > \omega_c$ increases, a significant number of the localized modes will be thermally excited and their

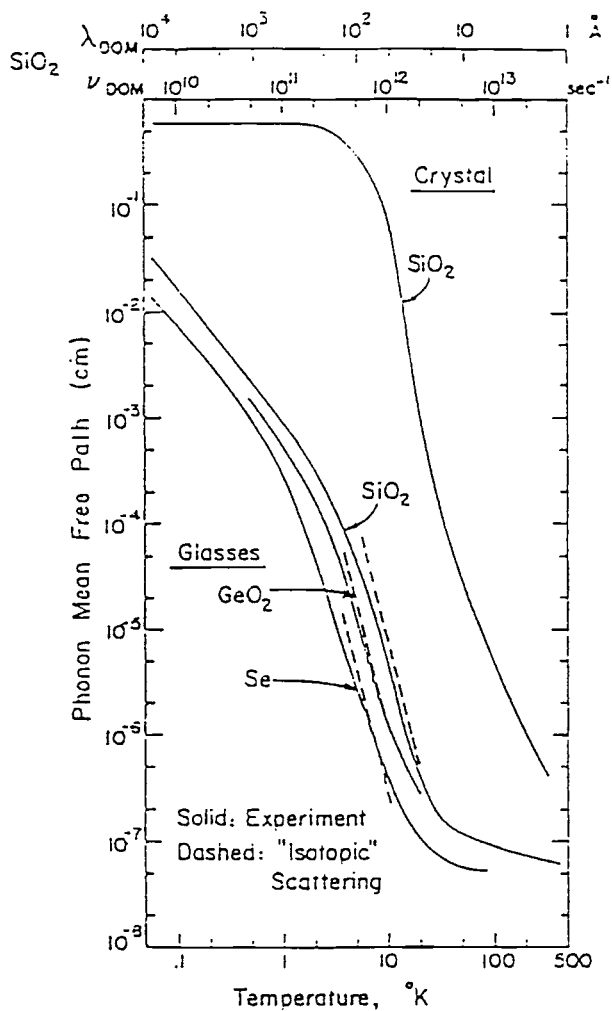


Figure 10. Average phonon mean free path as a function of temperature for various glasses and SiO_2 crystal (from ref. 12).

hopping will contribute to an increase in the thermal conductivity above the plateau value[12]. The scattering mechanism believed to be responsible is the three phonon anharmonic process where an extended phonon interacts with a localized phonon to produce another localized phonon. Alexander and coworkers[16] derived an expression for the contribution of this anharmonic process to the thermal conductivity. In their derivation, they assumed glasses are fractal, and through a fracton-hopping formulation introduced an additional heat-carrying channel above the plateau, which generated a linear increase in thermal conductivity with increasing temperature. Though they assumed a fractal nature for glasses, Graebner and coworkers[10] point out, that in addition to the lack of evidence of the fractal nature of bulk glass, the assumption is not needed to explain the phonon assisted hopping of the localized modes above the plateau.

Statement of Purpose

The purpose of this experiment was to track the effect of europium doping on the baseline composition of a set of aluminosilicate glasses as it is inserted into the network in greater quantities. Specifically, as the molar fraction of europium increased from one sample to another, the thermal diffusivity as a function of temperature was examined in the temperature range of 100-500^oC. The data was analyzed using a two-carrier model for thermal transport by extended phonons, and thermally activated hopping of localized phonons. Within the two-carrier model, a Debye approximation is used to calculate the heat capacity of the extended modes, while a multi-term Einstein approximation using vibrational modes obtained from Raman data is used to calculate the total heat capacity of the samples.

CHAPTER II

EXPERIMENTAL PROCEDURE

Samples

The five samples studied were europium doped aluminosilicate glass samples prepared by L. Pierre de Rochemont of C²Technologies. The compositional variation of the europium varies as (Base Composition)_{1-x}(Eu₂O₃)_x, with the base composition being 0.70-SiO₂--0.03-Al₂O₃--0.12-MgO--0.15-Na₂O. The europium molar fractions for these glasses ranged from 0.1% to 5.0% and are listed in table 1. The molar fraction of europium was added into the base composition in amounts that varied linearly with sample density. Since the volume of the samples were approximately equal, figure 11 displays the molar mass instead of the density, of the samples as a function of europium concentration. The dimensions of the samples were approximately 14mmx4mmx4mm. Three grooves approximately 30 μm in width were cut into the samples 4mm apart for the placement of the thermocouples.

Experimental Setup

The experiment was conducted under microcomputer control with instruments communicating over an IEEE-488 interface bus. The instrumentation consisted of three Hewlett-Packard model 3478A digital multimeters having a sensitivity of 0.1μV, a Hewlett-Packard model 3421A data acquisition/control unit, and a Hewlett-Packard 6284A dc power supply. The thermocouples which were anchored to the sample with a small amount of thermally conducting paste (an alumina-filled silicone grease), were 0.003in diameter chromel-alumel thermocouples referenced to electronic ice points manufactured by Omega Engineering. For measurements above room temperature, the

Composition I.D.	Eu ₂ O ₃ (mol%)	Base Composition (mol%)
Bragg-5	0	100
Bragg-6	0.1	99.99
Bragg-7	0.5	99.95
Bragg-8	1.0	99.00
Bragg-9	2.5	97.50
Bragg-10	5.0	95.00

Table 1. Sample Composition

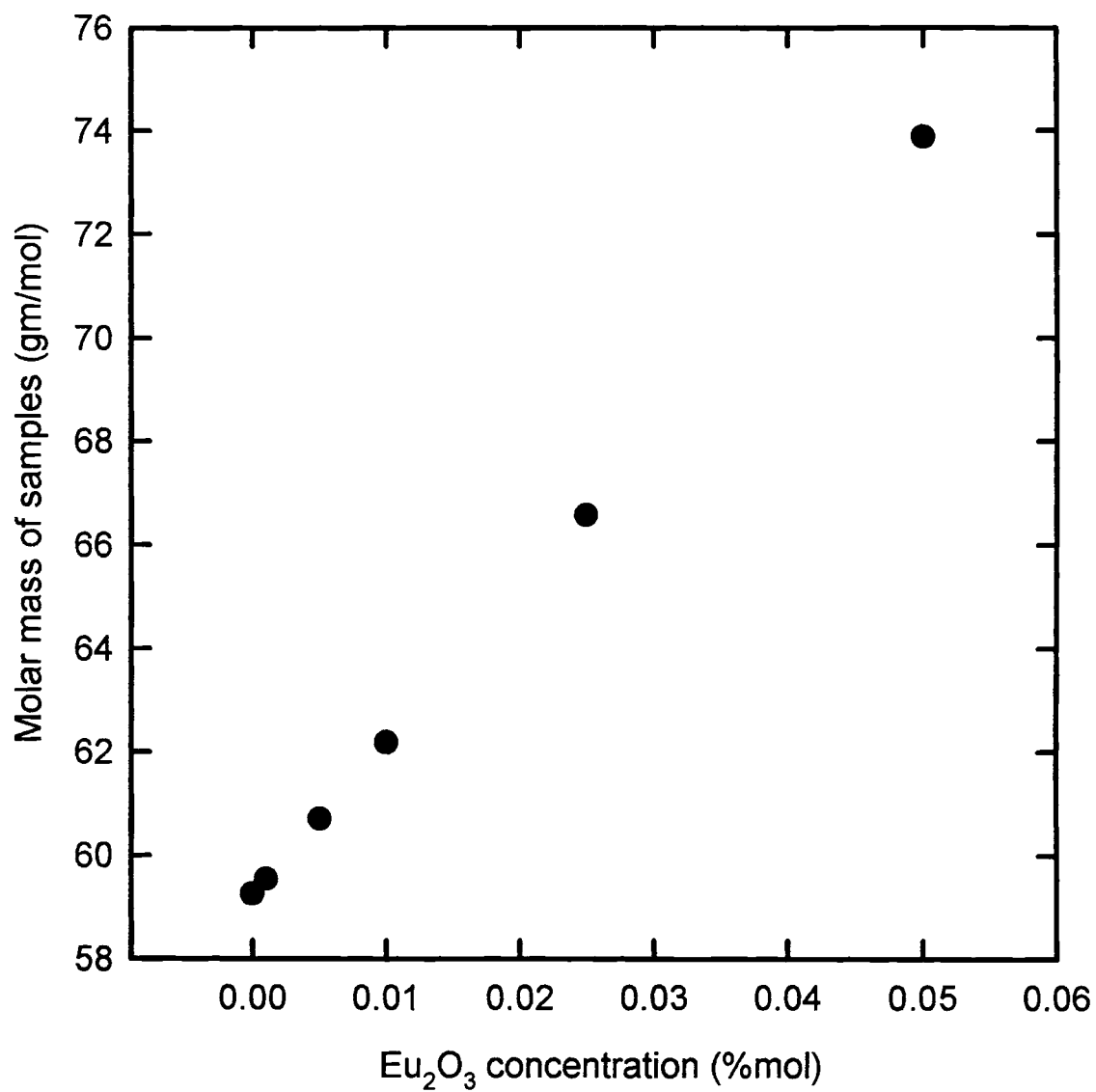


Figure 11. Molar mass of the samples vs. europium concentration.

samples were mounted using the same thermal compound mentioned above, in a small tube furnace that controlled the mean temperature of the sample. For low temperature measurements the sample was mounted on the cold finger of a liquid nitrogen cryostat. The base onto which the sample was mounted was attached to a resistance heater used to obtain a transient temperature distribution in the sample. Figure 12 illustrates a block diagram of the experimental setup. The section of the cryostat containing the sample is shown enlarged for clarity.

Procedure

Rather than measuring the thermal conductivity as a function of temperature, which is what has traditionally been measured in studies concerning thermal transport properties in solids, the thermal diffusivity was measured as a function temperature. Measuring the thermal diffusivity has the advantage that it is insensitive to radiative heat losses when dealing with poor thermal conductors[3]. Thermal diffusivities were measured using a similar set up of the transient method developed by Kennedy and coworkers[3]. During each experimental run, simultaneous readings of the three thermocouples were obtained by sending a group trigger command to the digital multimeters. With the sample in steady-state conditions temperature readings were taken to establish a “baseline” for the measurement. On command from the computer, the digital relay was closed, supplying current to the resistance heater. A constant current was maintained and a 10 s delay was allowed to give the thermocouple farthest away from the resistance heater time to respond. After the delay, simultaneous temperature measurements were taken by the three thermocouples at intervals of 0.5 s for a total time

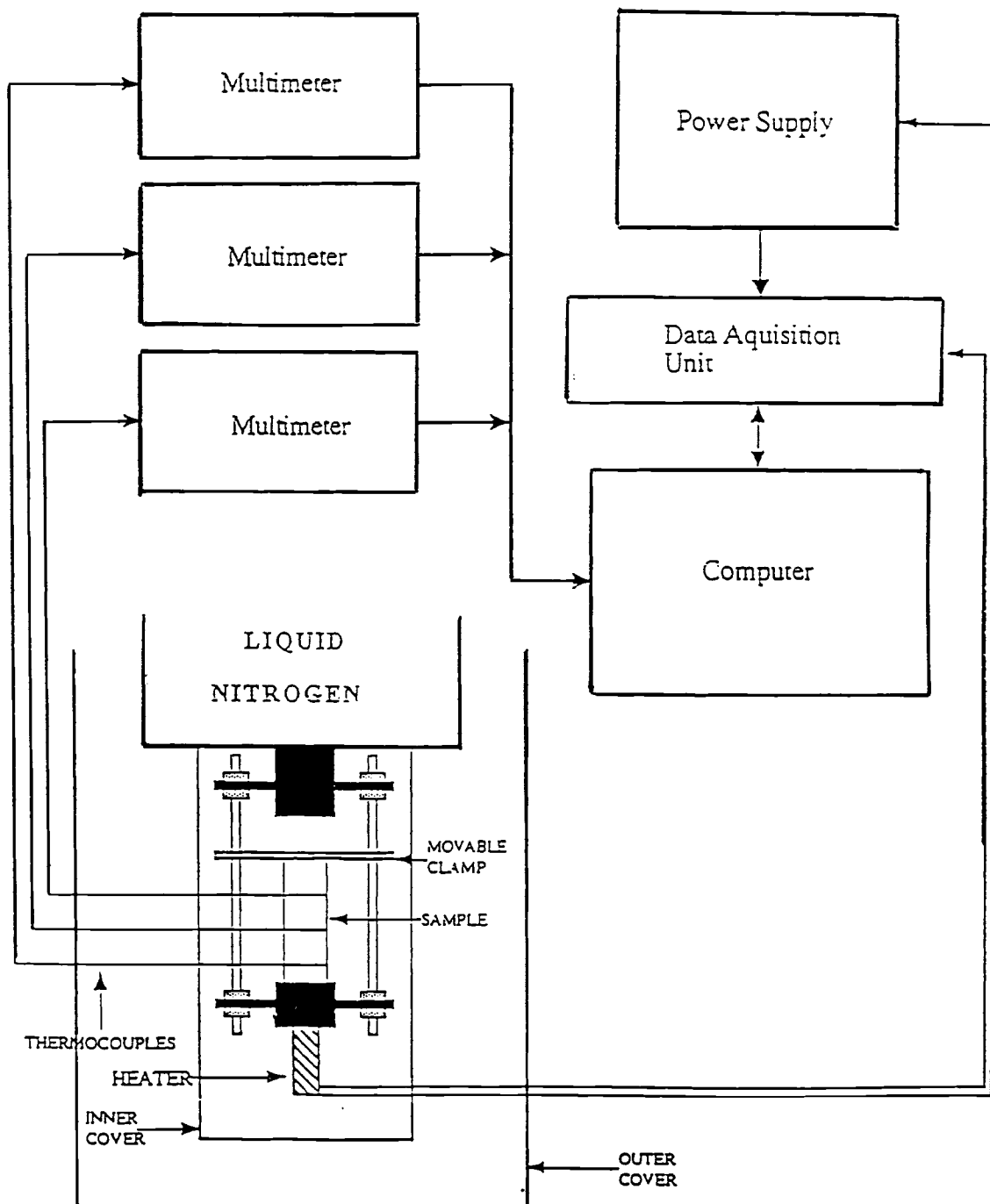


Figure 12. Schematic representation of the experimental setup.

of 50 s. During each experimental run a temperature change of approximately 3 to 8 K occurred at the thermocouple closest to the heater. At the end of each experimental run the relay was opened to turn off the heater and allow steady-state conditions to become re-established before the next run which occurred 30min later. The purpose for the 30min interval between experimental run was to ensure that the transients were given enough time to dissipate. Figure 13 displays a typical data set of temperature versus time for one of the samples.

The thermal diffusivity, α , was obtained from the data using the diffusion equation,

$$\partial T/\partial t = \alpha \nabla^2 T \quad (1)$$

This equation was solved for the diffusivity by the computer using a simple algorithm.

Under the assumption of one dimensional heat flow, $\nabla^2 T$ was estimated by the finite difference relation

$$\nabla^2 T_M \approx [(T_U - T_M) - (T_M - T_L)] / (\Delta x)^2 \quad (2)$$

for each measurement time in the data set[3]. The subscripts L,M,and U refer to the lower, middle, and upper thermocouples, respectively, while Δx is the spacing between adjacent thermocouples. At each time t_j , $\partial T(t_j)/\partial t$ was estimated by fitting a regression line to a short segment consisting of approximately eight points of $T_M(t)$ on either side of t_j and using the slope of this line as the estimate of the time derivative. The estimates of $\nabla^2 T_M$ were refined by averaging over the same time interval used to evaluate the time derivative[3]. Based on equation (1), $\partial T_M/\partial t$ should be a linear function of $\nabla^2 T_M$ with slope α . Figure 14 shows the result of this procedure applied to the data set shown in figure 13. As can be seen the curve is approximately linear. The thermal diffusivity, α , was then assigned to the mean temperature of the middle thermocouple during each

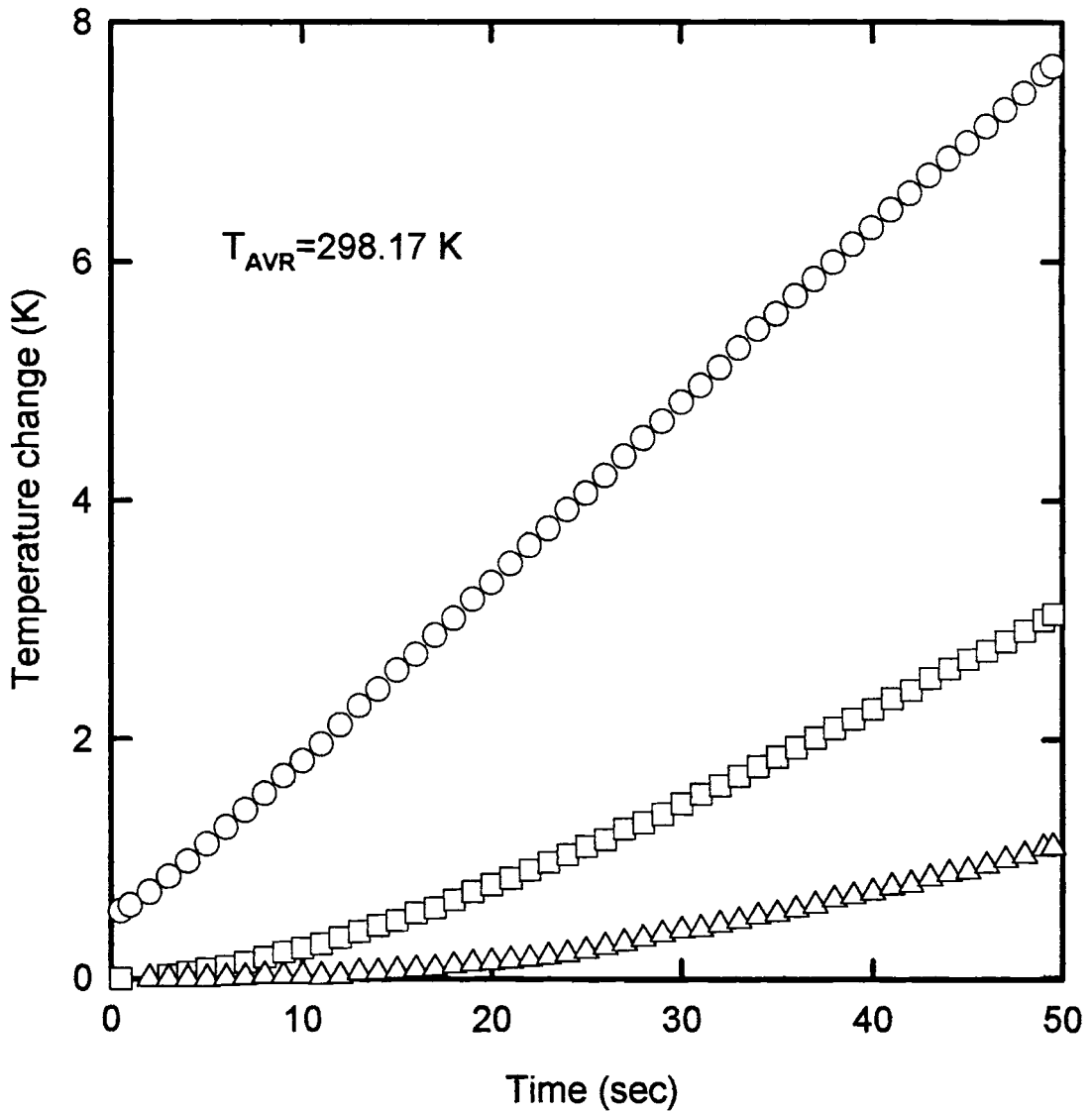


Figure 13. Typical temperature vs. time data. The upper curve is for the thermocouple closest to the heater and the lower curve is for the thermocouple farthest away from the heater.

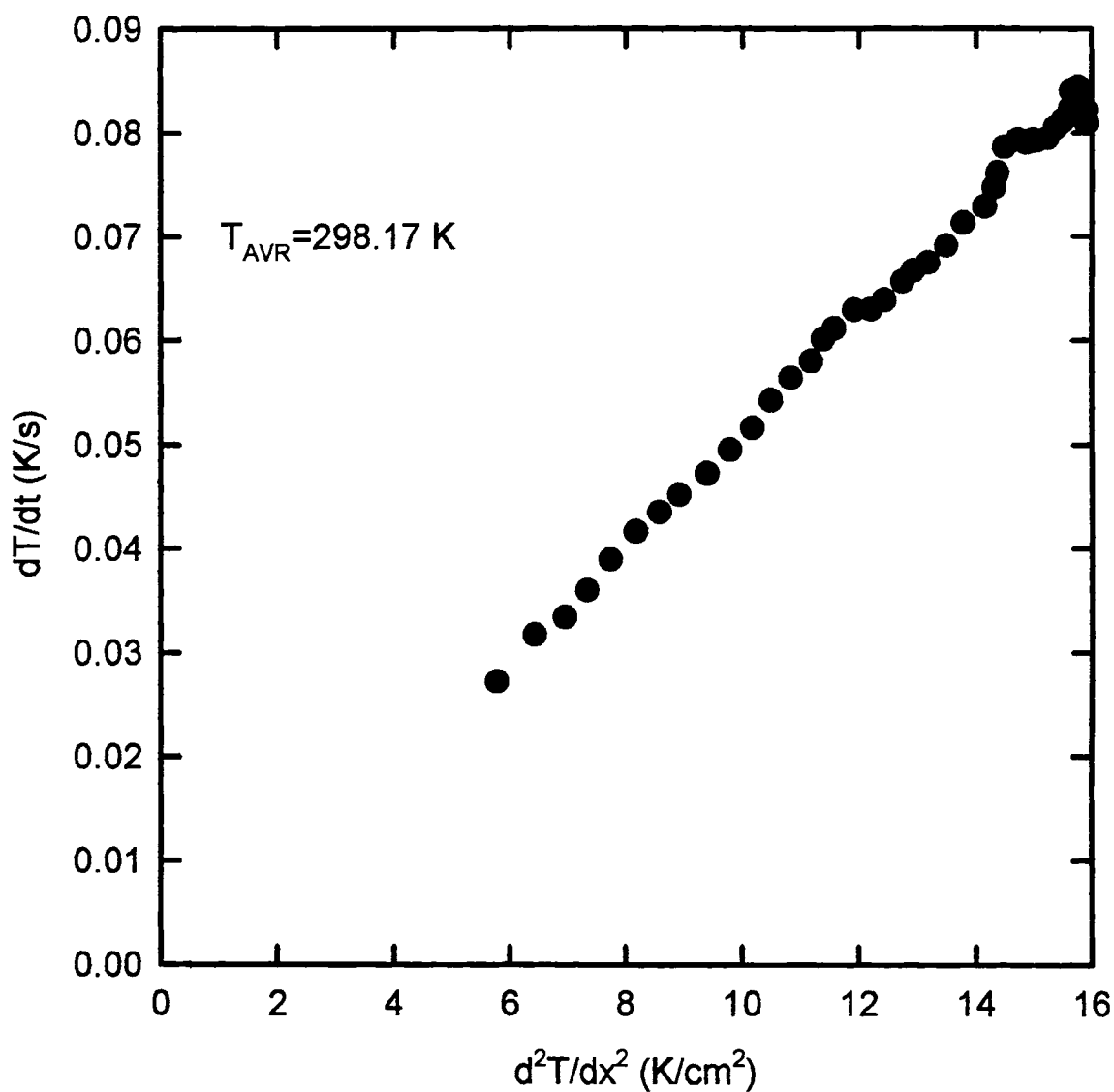


Figure 14. Plot of $\partial T/\partial t$ vs. $\partial^2 T/\partial x^2$ calculated from the data of figure 13. The slope of this curve is the thermal diffusivity, α .

experimental run. The experimental setup and procedure used in this experiment was exactly that used by Dixon and coworkers[3]. According to ref. 3 two kinds of checks were performed to determine the reliability of the algorithm used to measure thermal diffusivity. Based on these checks the method was deemed reliable.

CHAPTER III

RESULTS and DISCUSSION

The thermal diffusivities of the six samples studied are shown as a function of temperature in figures 15-20. Figure 21 displays the diffusivity of the samples on a single graph. As can be expected the curves are all very similar in form with the uppermost curve representing the sample with no europium and the lowermost curve representing the sample with the highest europium concentration. Within experimental error we see that as the concentration of europium in the samples increases the thermal diffusivity decreases in this temperature range. In particular, the effect of the europium is seen to be most prominent at the higher temperature limit. It will be demonstrated below that not only does the model of thermal transport by thermally activated hopping of localized phonons fit the data well, but in addition, this model will also account for the stronger effect that the europium concentration has on the thermal diffusivity at higher temperatures.

The model used to describe the data is the model proposed by Dixon and coworkers[3,4] where thermal transport is represented by a two-carrier model of conventional phonon-gas transport by extended phonons and thermally activated hopping of localized phonons. In this model, the extended phonons produce a transport that is a decreasing function of temperature between 100 and 250K, while the localized phonons produce a transport that is a linearly increasing function of temperature above 250K[4]. While this model employs many of the ideas inherent in the fracton model proposed by Orbach and coworkers[9,11,12], it differs in that a fractal nature of glasses is not assumed. Instead, empirical properties of the glasses are used to support the analysis.

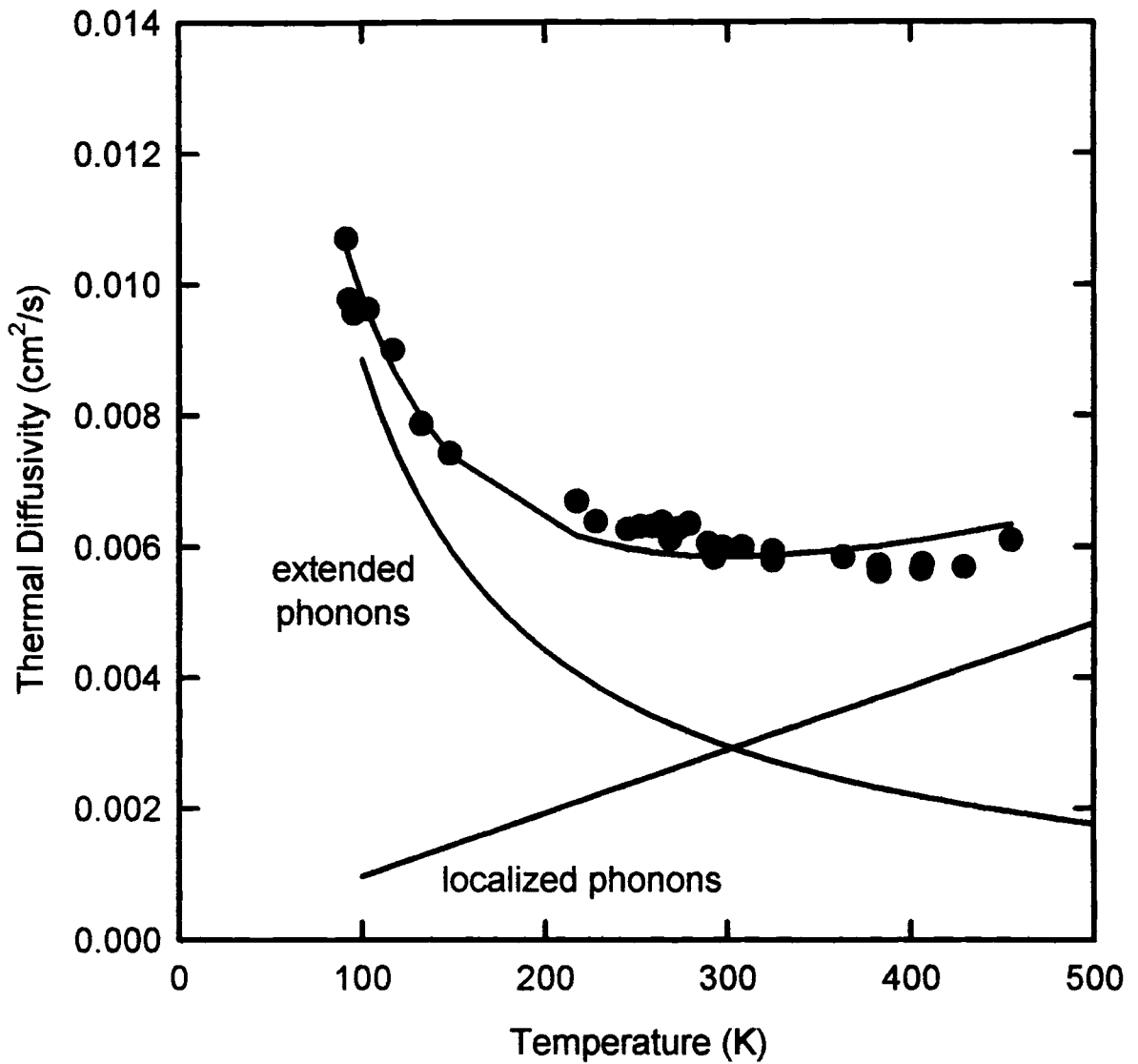


Figure 15. Thermal diffusivity as a function of temperature for the Bragg5 sample. In addition, the individual contributions to the thermal diffusivity of the extended and localized phonons is shown.

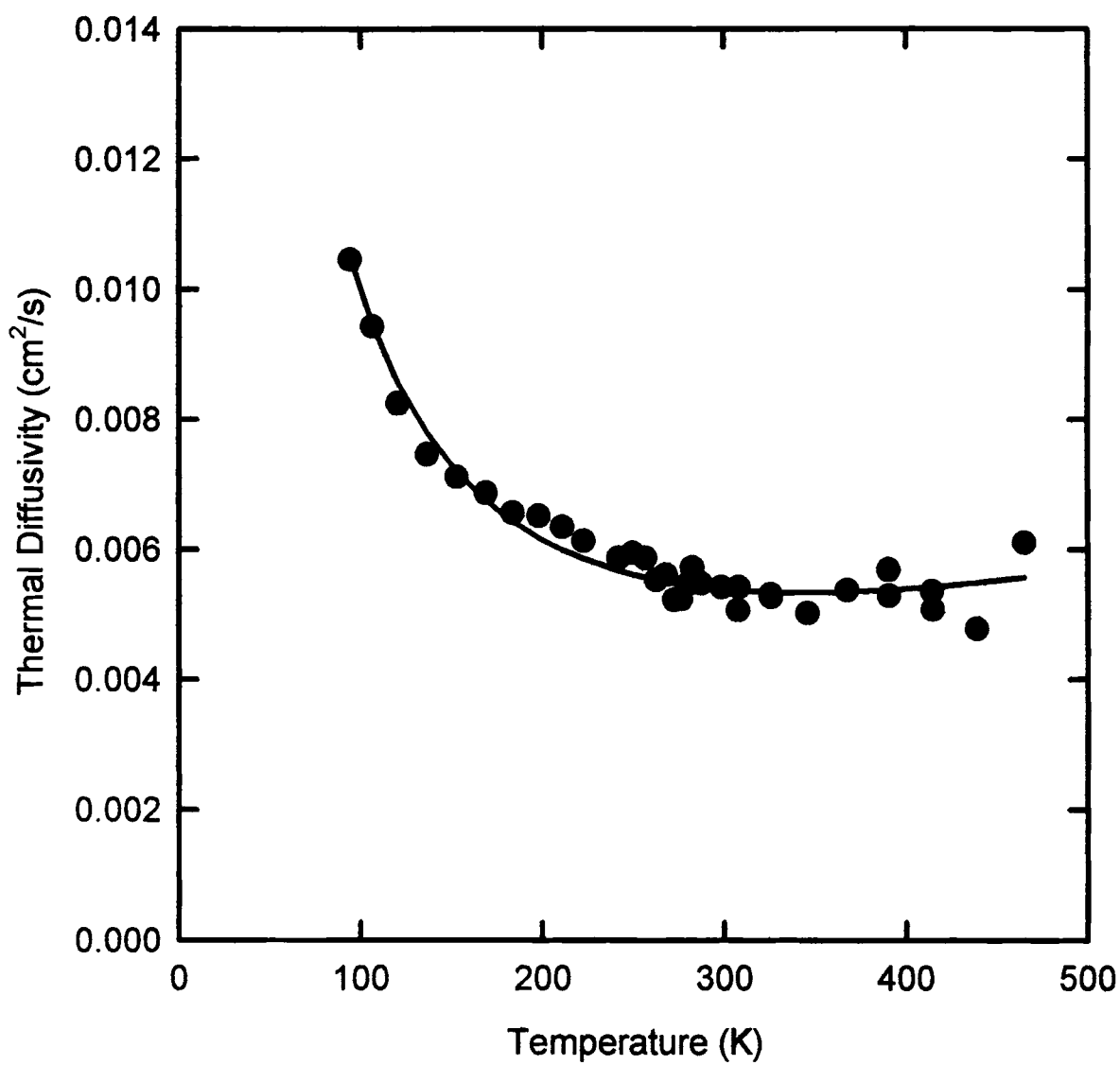


Figure 16. Thermal diffusivity as a function of temperature for the Bragg6 sample.

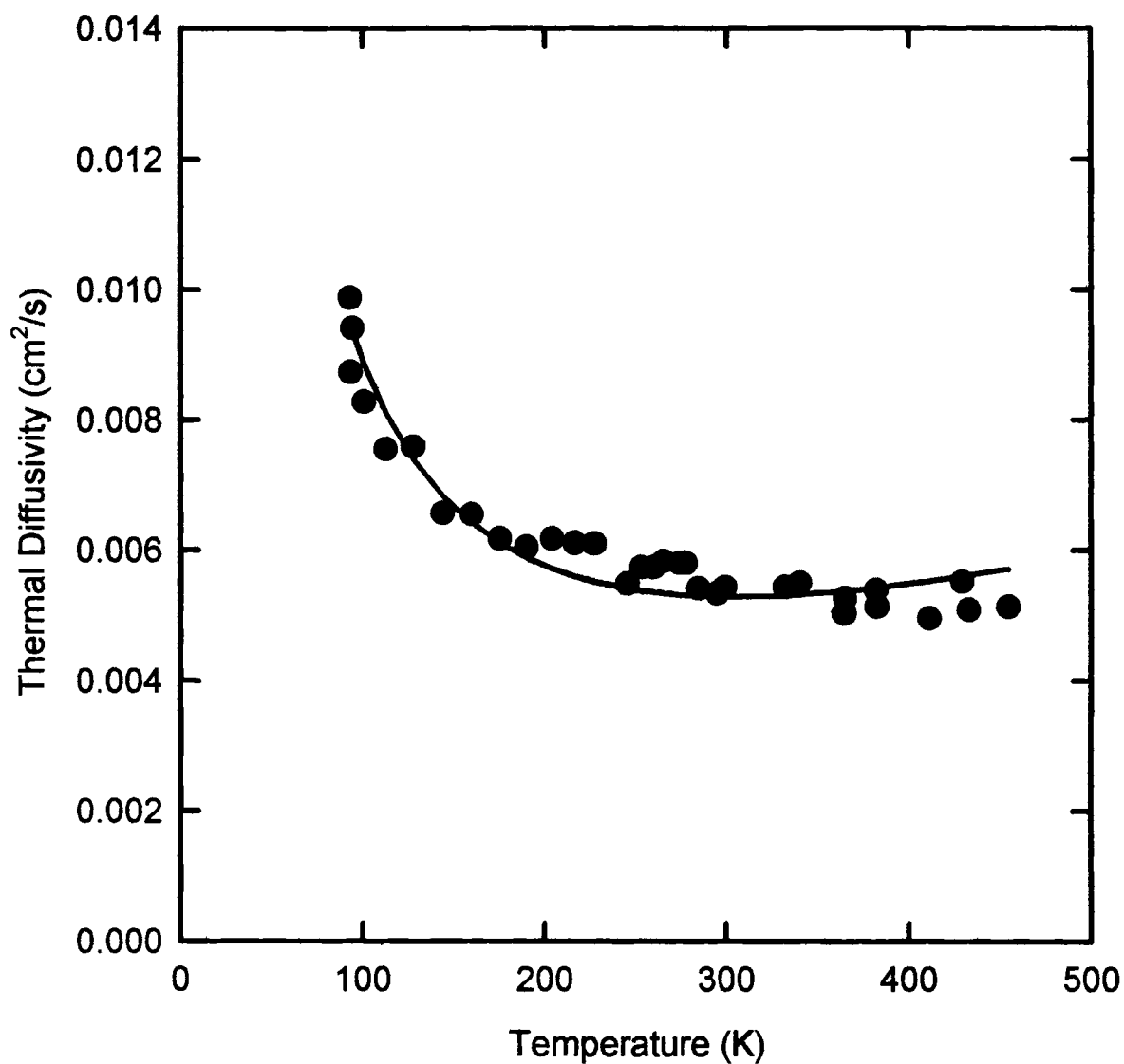


Figure 17. Thermal diffusivity as a function of temperature for the Bragg7 sample.

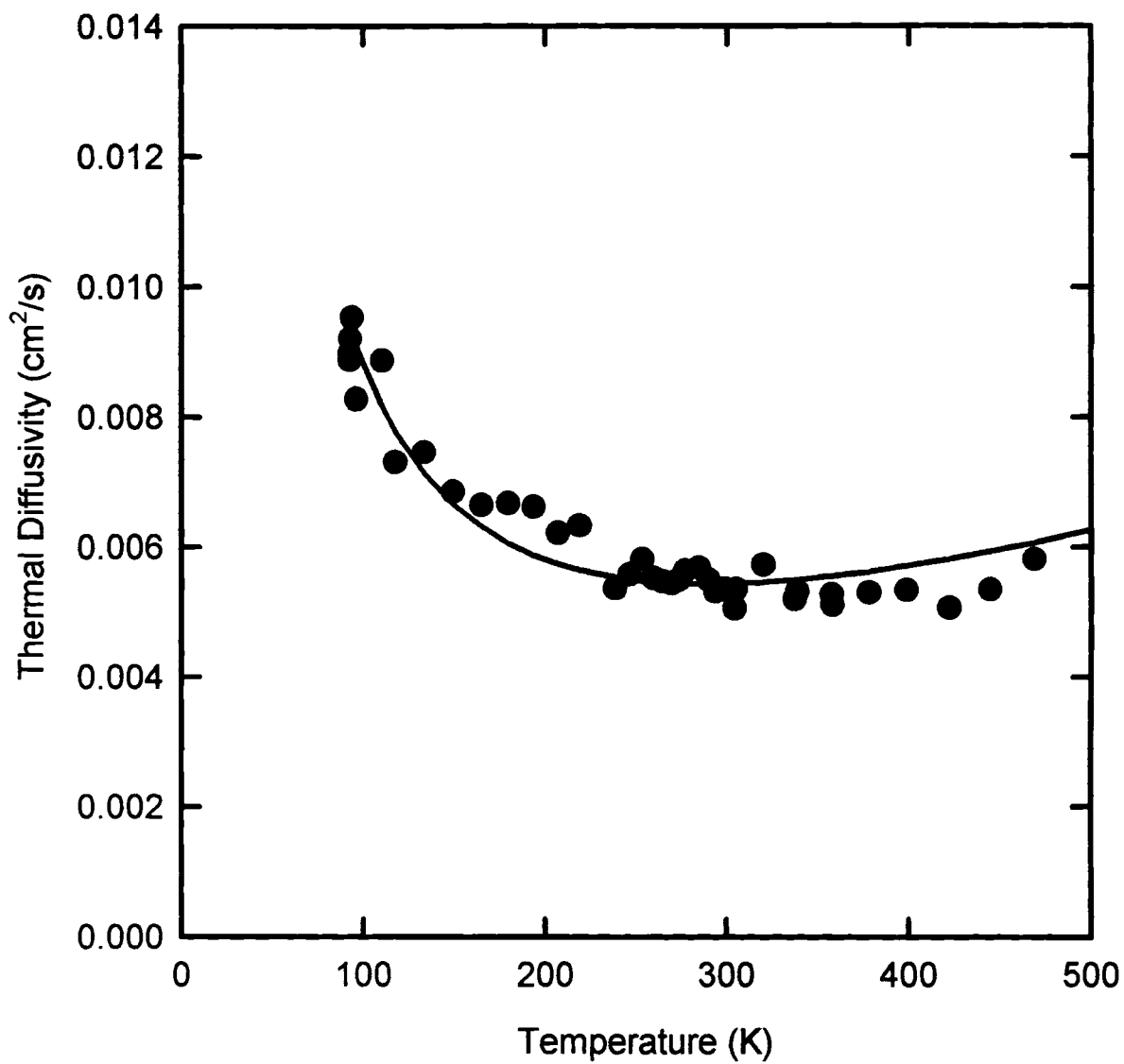


Figure 18. Thermal diffusivity as a function of temperature for the Bragg8 sample

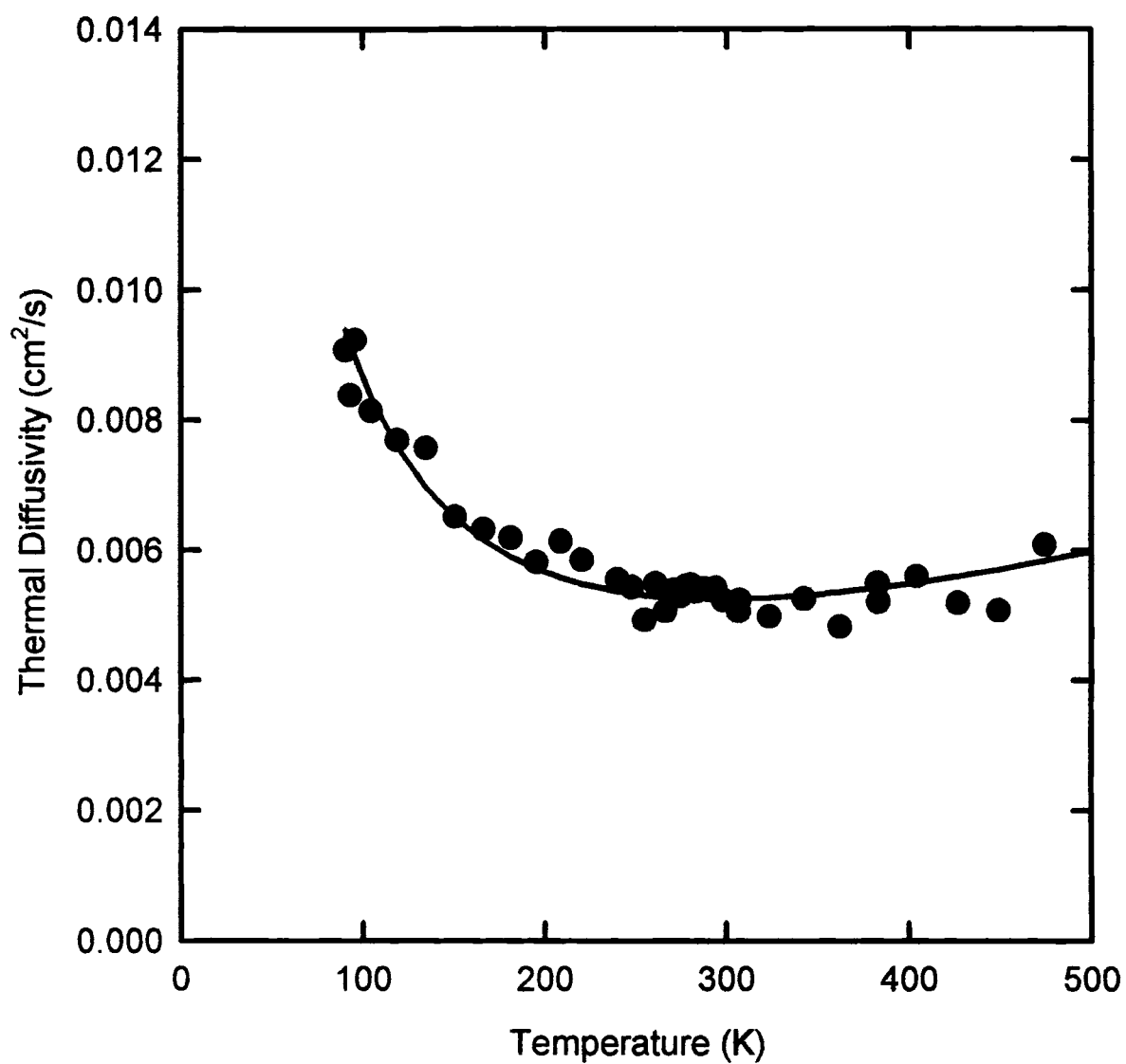


Figure 19. Thermal diffusivity as a function of temperature for the Bragg9 sample

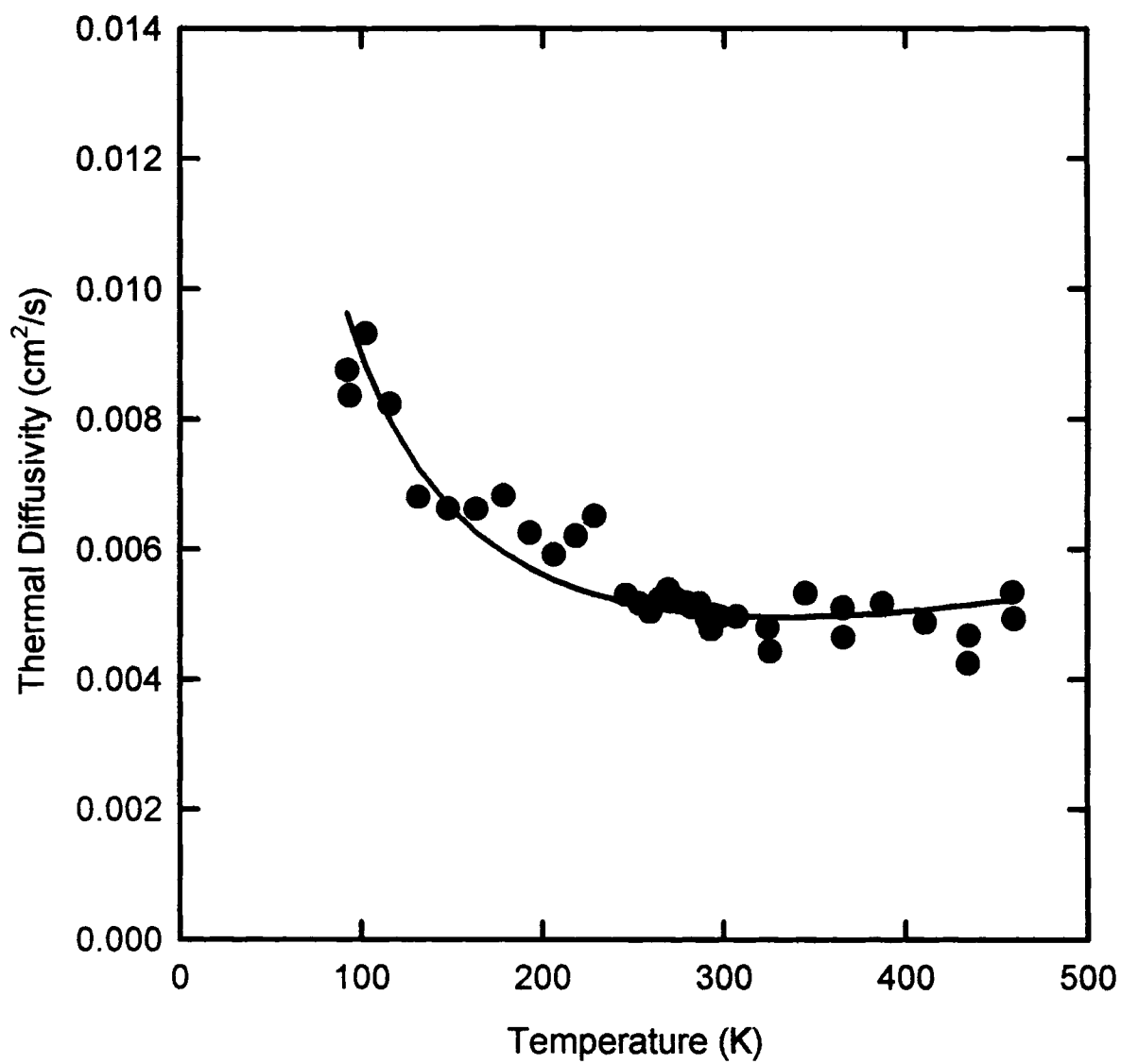


Figure 20. Thermal diffusivity as a function of temperature for the Bragg10 sample

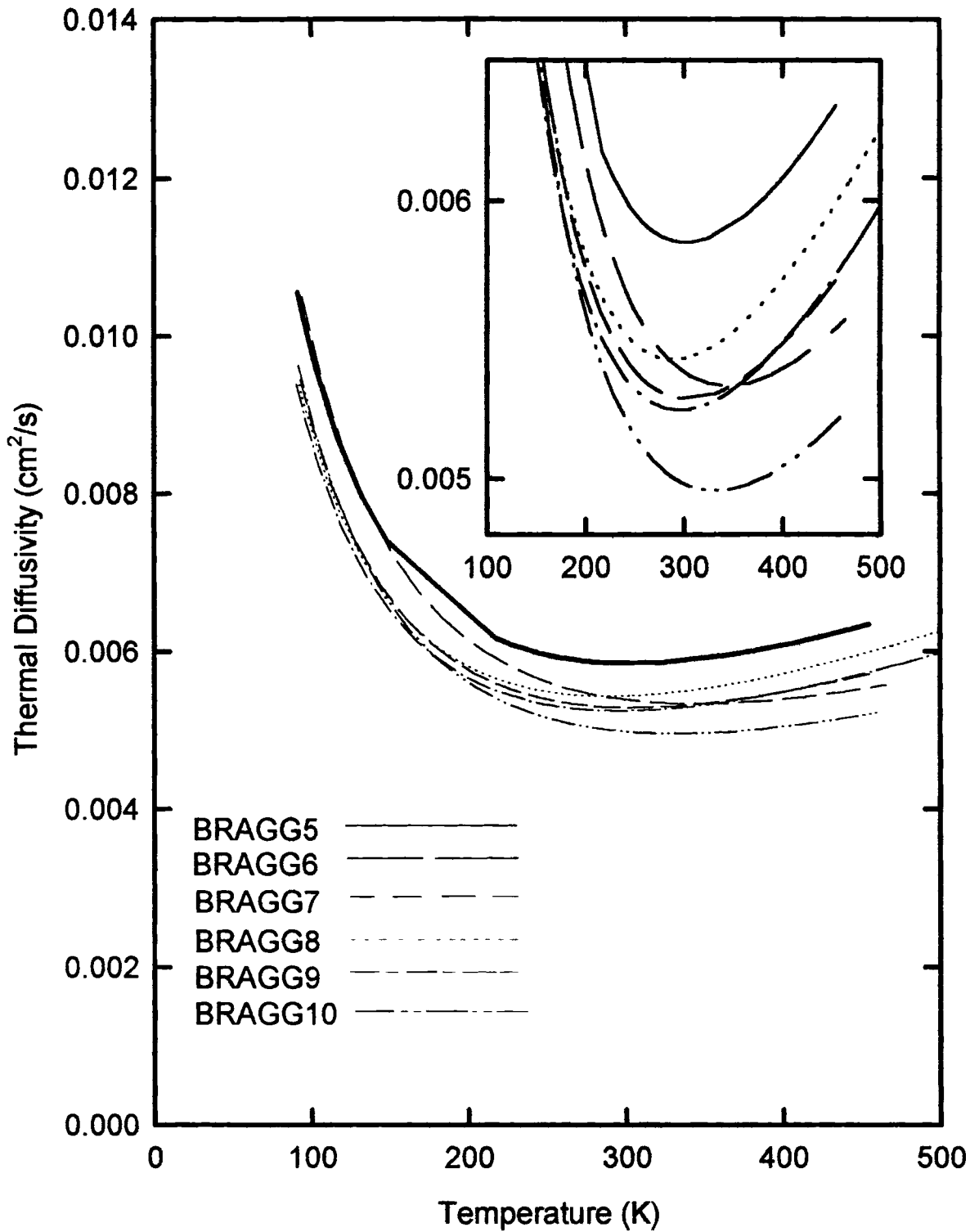


Figure 21. The thermal diffusivities as a function of temperature for all six samples. The caption in the upper right hand corner is the diffusivities in an expanded scale for clarity.

Table 2 lists the relevant physical properties of the glasses used in this analysis. In particular, the concept of a “formula unit” was employed. The formula unit was first introduced by Dixon and coworkers[3] and is defined as the smallest number of atoms in which each element is represented in the same proportion as in the sample as a whole. Since the glasses studied here are mixtures rather than compounds, the formula units are not whole numbers. The molar volume is the ratio of the mass of the formula unit to the density of the sample. Table 2 also includes the velocity of sound in the samples studied. Due to the lack of sound velocity measurements for these glasses, a value of $3.88 \times 10^5 \text{ cm/s}$ was used for all six samples. This value was taken from a sample in ref. 4 which was very similar in composition to the Bragg10 sample in this experiment.

The existence of low frequency extended phonons and localized phonons was inferred from Raman scattering experiments previously conducted on the samples studied in this experiment. The Raman spectra for the samples is shown in figures 22 to 27. The onset of Raman activity is taken as representing phonon localization with the cutoff frequency, ω_c , separating the extended phonons from the localized ones[3]. While Dixon and coworkers[3,4] interpret the boson peak in the Raman data as representing the mobility edge (cutoff frequency), in this experiment the minimum preceding the boson peak is taken as representing the mobility edge. The mobility edge for the Bragg5 sample which has no europium occurs at a frequency of 15 cm^{-1} , while for the other five samples, it occurs at a frequency of 12 cm^{-1} . This shift in the mobility edge from a larger frequency (or smaller wavelength) to a smaller frequency (or larger wavelength) may be attributed to the fact that the europium increases the length scale of the disorder in the glasses causing the extended phonon wavelength to approach the length scale of the disorder in the glass

	BRAGG5	BRAGG6	BRAGG7	BRAGG8	BRAGG9	BRAGG10
Formular Number	294	294.2	295.9	296.1	299.2	304.3
Formula Mass (u)	5580	5959	6076	6222	6661	7392
Density (g/cm ³)	2.21	2.24	2.29	2.27	2.4	2.55
Molar Volume (nm ³)	4.19	4.42	4.41	4.54	4.63	4.82
Sound Velocity (10 ⁵ cm/s)	3.88	3.88	3.88	3.88	3.88	3.88
ω_c (cm ⁻¹)	15	12	12	12	12	12
Raman Frequencies (cm ⁻¹)						
ω_1	83	76	76	76	76	76
ω_2	470	493	463	433	433	435
ω_3	575	590	580	583	590	607
ω_4	791	787	783	783	783	787
ω_5	962	959	949	949	949	959
ω_6	1096	1098	1095	1089	1086	1076
C (J/K-cm ³)	8.43	7.91	8.12	7.98	7.9	7.64
C_{ext} (10 ⁻⁴ J/K-cm ³)	2.71	1.39	1.39	1.39	1.39	1.39
C_{ext}/C (10 ⁻⁵)	3.21	1.75	1.71	1.74	1.75	1.81
B (10 ⁻⁶ cm ² /s-K)	9.66	7.73	8.66	9.36	8.84	7.46
A (10 ⁴ cm ² K/s)	2.76	5.26	4.73	4.54	4.44	4.54

Table 2. Physical properties of the glasses.

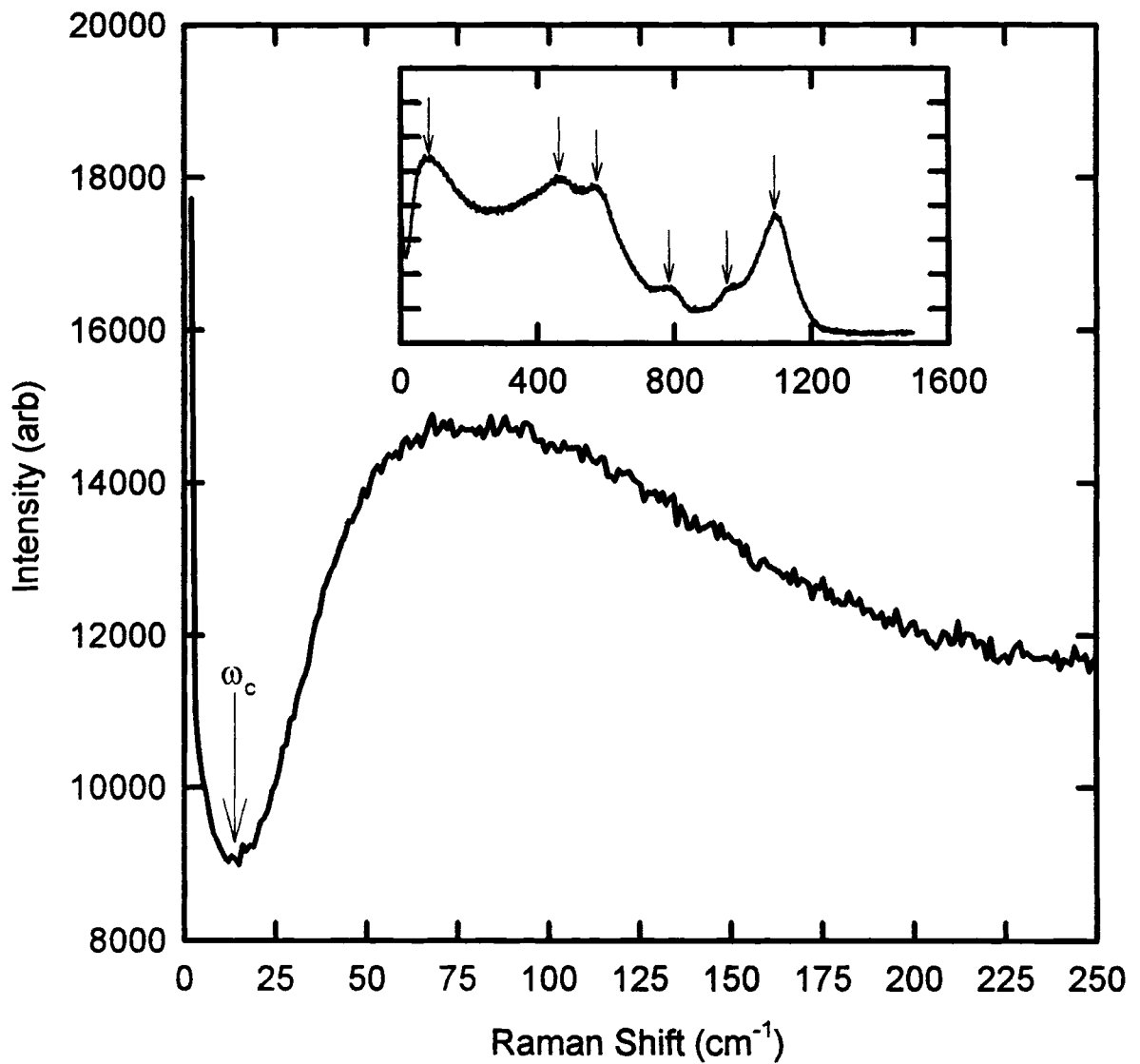


Figure 22. Raman spectrum of the Bragg5 sample. The main figure shows the region of the mobility edge. The inset shows the full Raman spectrum for this sample. The arrows in the full spectrum point to the frequencies used in the multi-term Einstein approximation.

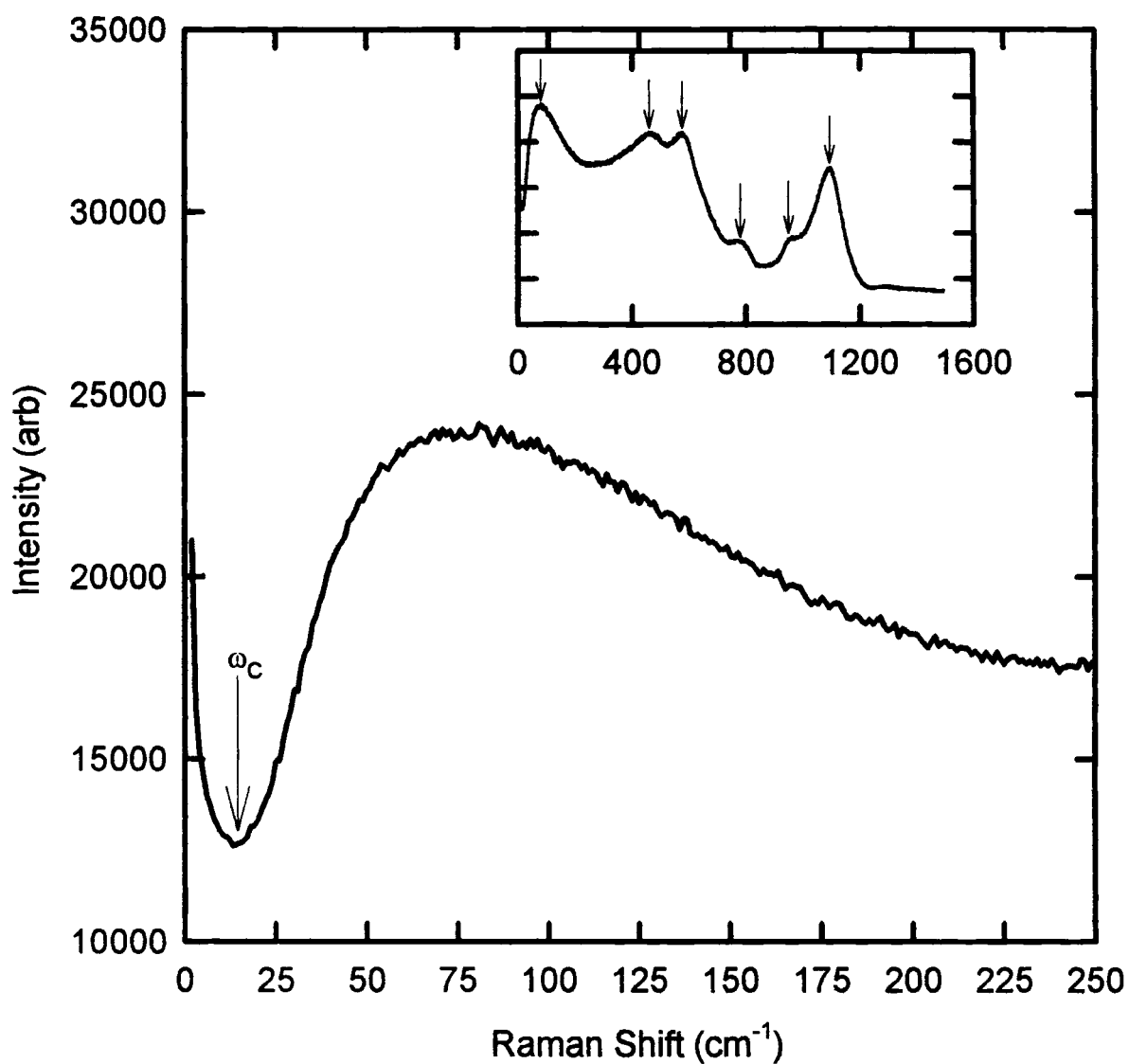


Figure 23. Raman spectrum of the Bragg6 sample. The main figure shows the region of the mobility edge. The inset shows the full Raman spectrum for this sample.

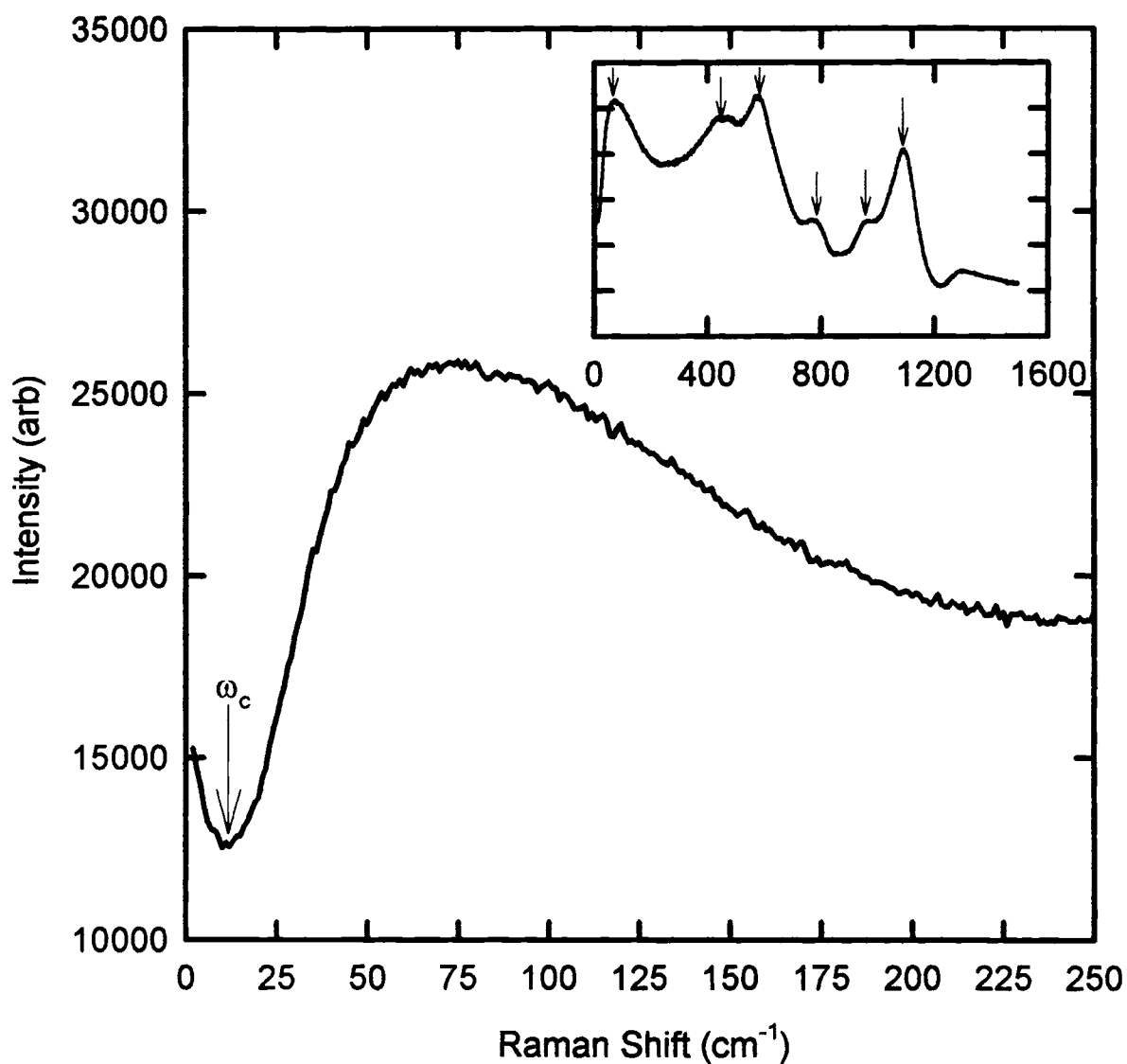


Figure 24. Raman spectrum of the Bragg7 sample. The main figure shows the region of the mobility edge. The inset shows the full Raman spectrum for this sample.

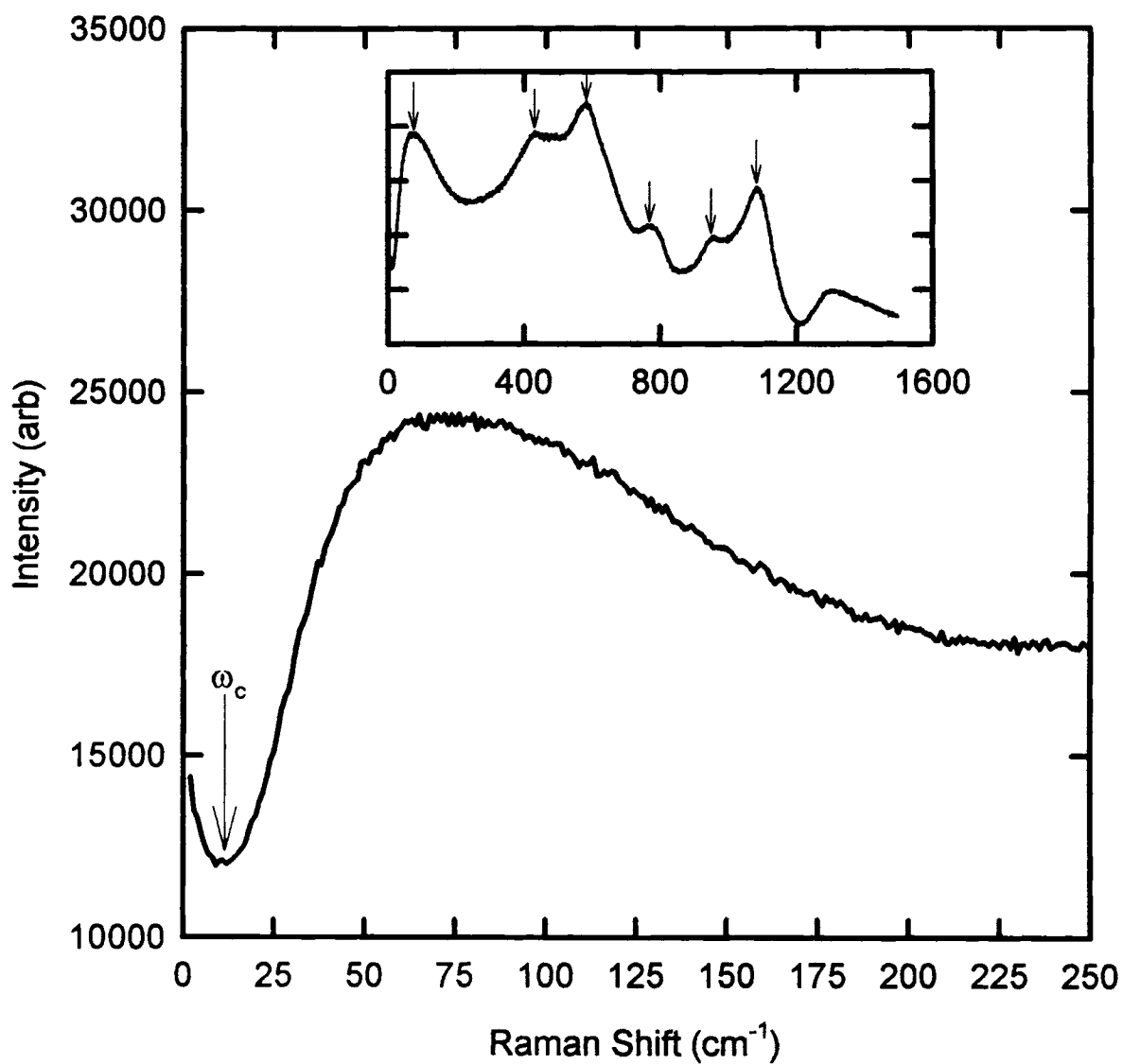


Figure 25. Raman spectrum of the Bragg8 sample. The main figure shows the region of the mobility edge. The inset shows the full Raman spectrum for this sample.

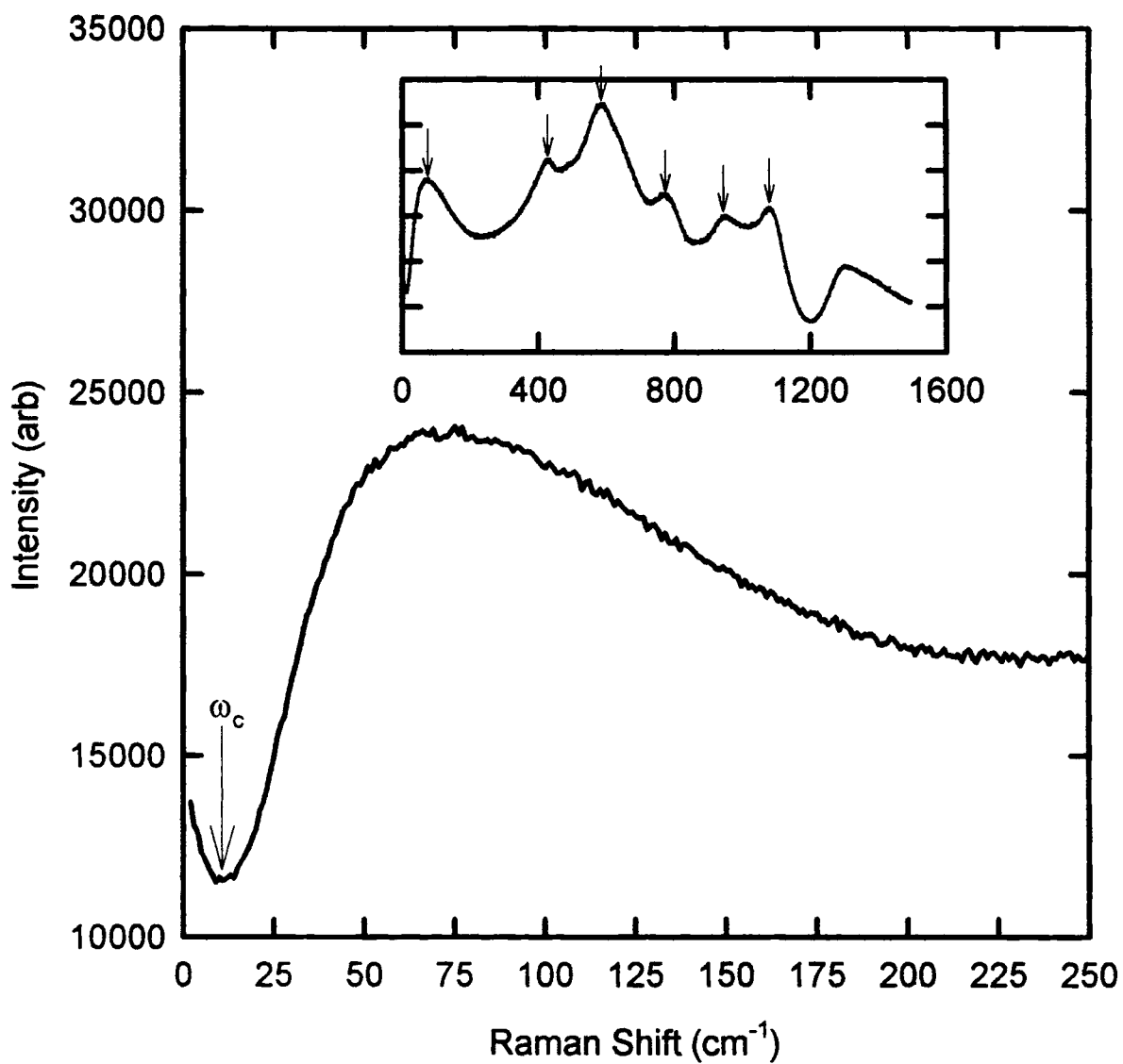


Figure 26. Raman spectrum of the Bragg9 sample. The main figure shows the region of the mobility edge. The inset shows the full Raman spectrum for this sample.

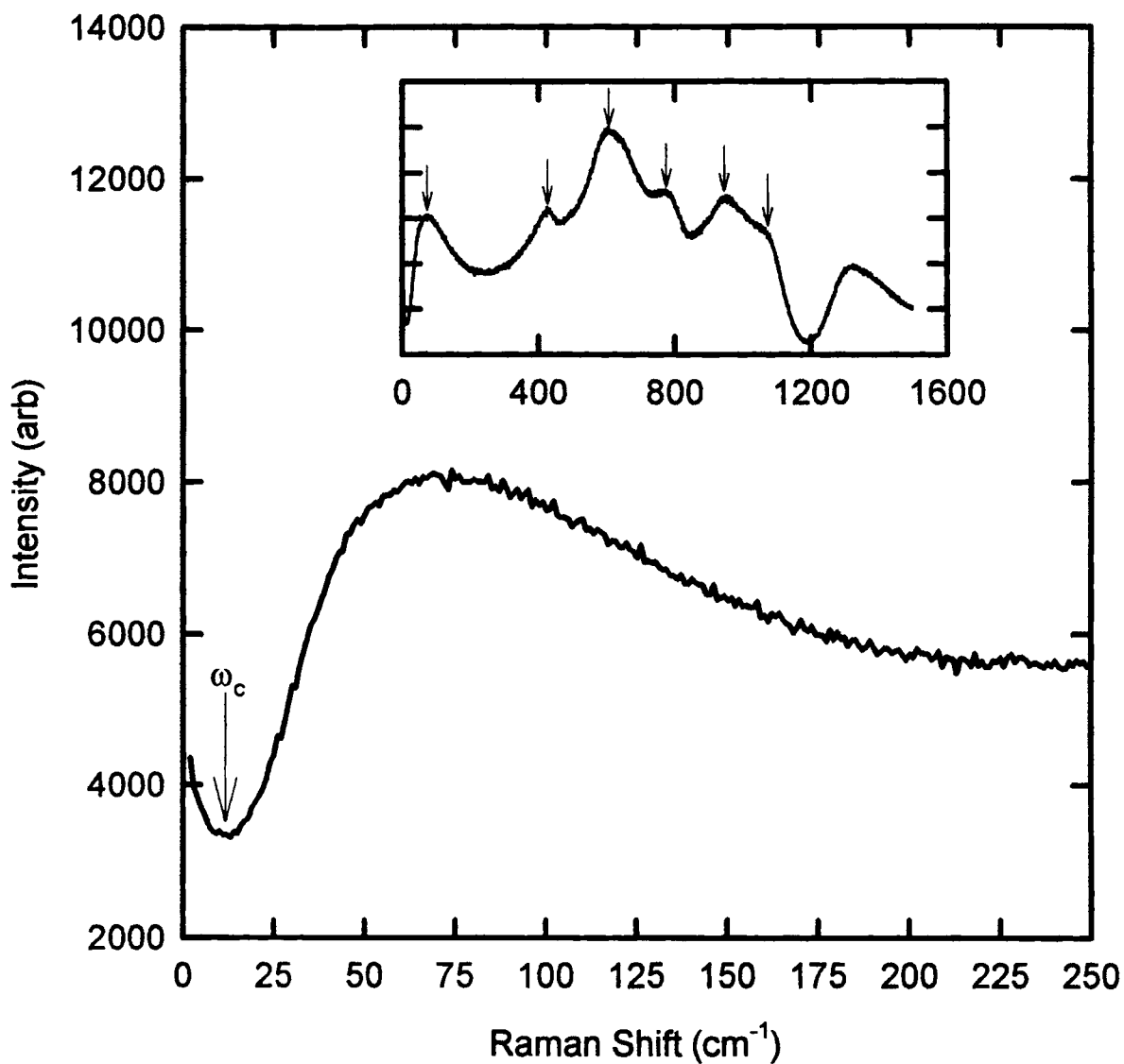


Figure 27. Raman spectrum of the Bragg10 sample. The main figure shows the region of the mobility edge. The inset shows the full Raman spectrum for this sample.

sooner in the Bragg6-10 samples than in the Bragg5 sample hence scattering the extended phonons sooner. The fact that the mobility edge is the same for the samples with different amounts of europium concentration may be accounted for by assuming that beyond the initial amount of europium required to produce the additional scattering, further increases in europium concentrations have no additional effects, at least in the concentrations present in the samples studied here. The peaks beyond the mobility edge are taken to represent the frequencies of the localized modes present in the samples. In figures 22-27, these peaks are identified by the arrows in the full Raman spectrum captions in the figures. These frequencies in addition to the mobility edge are listed in table 2.

Based on the two-carrier model, the thermal diffusivity due to the extended phonons and the localized phonons can be written as

$$\alpha = \frac{1}{3} \frac{C_{\text{ext}}}{C} v_s^2 \tau_{\text{ext}} + \frac{C_{\text{loc}}}{C} \frac{\langle R^2 \rangle}{\tau_{\text{loc}}} \quad (3)$$

where the first term represents the contribution due to extended phonons and the second term the contribution due to the thermally activated hopping of localized phonons. C_{ext} and C_{loc} are the heat capacity per unit volume of the extended and localized phonons, respectively, and $C=C_{\text{ext}}+C_{\text{loc}}$. τ_{ext} and τ_{loc} are the mean lifetimes of the of the extended and localized phonons, respectively, and v_s is the velocity of sound in the samples. $\langle R^2 \rangle$ represents the thermally averaged square hopping distance. Replacing C_{loc} with $C-C_{\text{ext}}$, equation (3) becomes

$$\alpha = \frac{1}{3} \frac{C_{\text{ext}}}{C} v_s^2 \tau_{\text{ext}} + \left(1 - \frac{C_{\text{ext}}}{C}\right) \frac{\langle R^2 \rangle}{\tau_{\text{loc}}} \quad (4)$$

If phonon-phonon scattering is assumed to be the dominant resistive anharmonic process for the extended phonons then $\tau_{\text{ext}} \propto T^{-1}$ can be used to fit the data[3,4]. On the other

hand, the major contribution of the localized modes to the thermal transport is believed to occur through a three phonon anharmonic process where an extended phonon is scattered by a localized phonon to produce another localized phonon. This process may also occur in reverse where a localized phonon scattered by another localized phonon produces an extended phonon. In this process energy conservation dictates that if a localized phonon decays, it must reappear a distance R away in some other mode in the glass. This is the process referred to as “hopping” by Dixon and coworkers[3,4]. Since the disorder of the glasses leads to a distribution of localized phonon frequencies where neighboring modes will most likely vary in frequency, a low frequency extended phonon will be emitted or absorbed to make up the energy difference between the donor localized modes and the acceptor localized modes[3]. This three phonon anharmonic process is illustrated schematically in figure 28. Orbach and coworkers[9,11,12] have demonstrated through their fractal model that this three phonon process contributes a localized thermal diffusivity that is a linear function of temperature to the total thermal diffusivity, $\alpha = \alpha_{\text{ext}} + \alpha_{\text{loc}}$. Keeping this in mind and the assumption that $\tau_{\text{ext}} \propto T^{-1}$, the functional equation used to fit the data is

$$\alpha = \frac{C_{\text{ext}}}{C} AT^{-1} + \left(1 - \frac{C_{\text{ext}}}{C}\right) BT \quad (5)$$

where A and B are constants to be determined by the fit.

In determining the heat capacity of the extended phonons, a Debye approximation was used at the high temperature limit for these modes. This approximation gives the extended phonon heat capacity as

$$C_{\text{ext}} = \left(\frac{\omega_c}{v_s}\right)^3 \frac{k_B}{(2\pi^2)} \quad (6)$$

Since the peaks in the Raman spectra extend to roughly 1100cm^{-1} , a multi-term Einstein

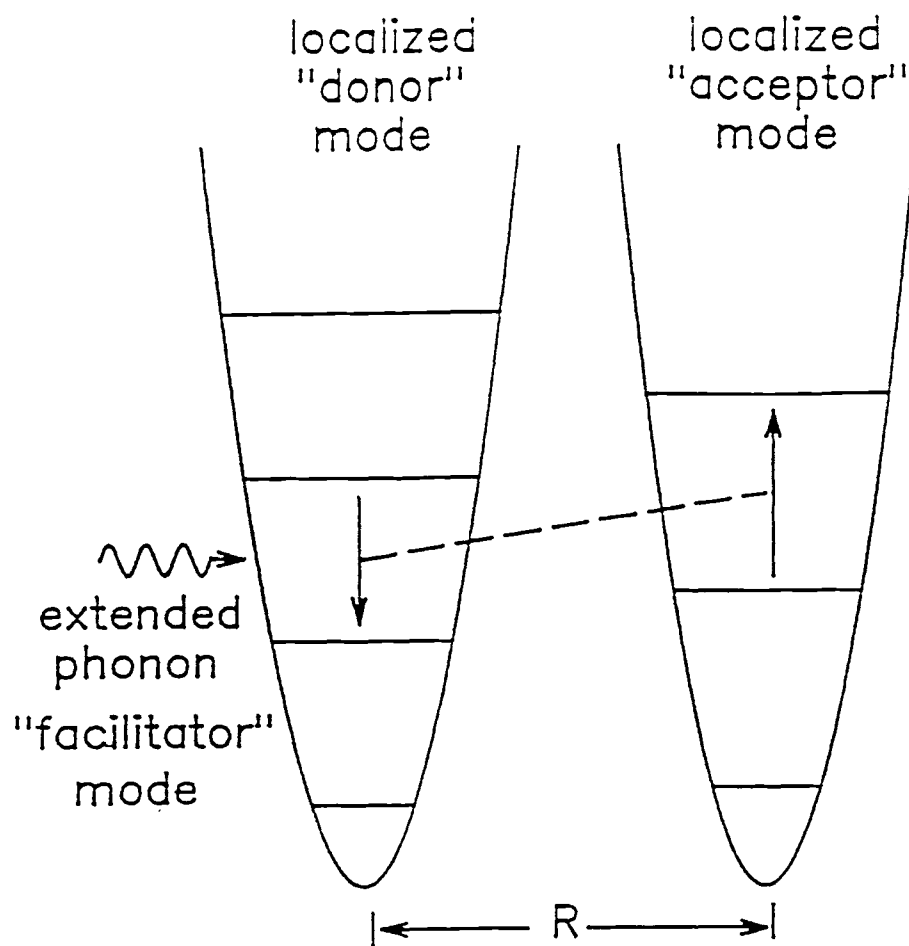


Figure 28. Schematic representation of the thermally activated hopping of localized phonon process.

approximation was used for the determination of the total heat capacity, C , to correct for the temperature variation of this total heat capacity. This was done by approximating the phonon density of states by the center frequencies of the six Raman peaks and substituting these frequencies in the equation

$$C = 3nk_B \left(\frac{h}{k_B T} \right)^2 \sum_{i=1}^6 \left(\frac{\omega_i^2 e^{h\omega_i/k_B T}}{(e^{h\omega_i/k_B T} - 1)^2} \right) \quad (7)$$

where n , the number of modes per unit volume was taken as the ratio of the formula unit to the molar volume and T was set equal to 300K, the high temperature limit for the extended phonons. The values for C , C_{ext} , and the ratio C_{ext}/C together with the constants A and B are listed in table 2. It is worth mentioning, that had the mobility edge been approximated by the boson peak in the Raman spectra as was done in [3,4], the values for the ratio C_{ext}/C calculated would have been similar to the values calculated for the families of glasses studied in [3,4]. Figure 15 displays the individual contributions of the extended and localized phonons to the thermal diffusivity of the Bragg5 sample, with similar curves applying to the other five samples.

In examining the thermal diffusivities in figure 21, it is seen that while at room temperature and above the thermal diffusivities increase linearly with temperature, for temperatures below room temperature the thermal diffusivities are a decreasing function of the temperature. This behavior is similar to that found in [4] for the family of glasses studied there. This is to be expected since the samples studied in this experiment are very similar to one of the samples studied in [4]. This is to be contrasted to the behavior of the thermal diffusivities of the family of glasses studied in [3], where the thermal diffusivities are roughly linear in temperature throughout the whole temperature region studied here

and in [3] and [4]. The fact that the extended phonons in the samples studied here and in [4] is seen to make a larger contribution relative to the localized phonons to the thermal diffusivity was suggested by Dixon and coworkers[3,4] to be due to weaker anharmonic interactions in these samples compared to stronger anharmonic interactions in the samples studied in[3]. The weaker anharmonic interactions in the glasses studied here and in [4] is assumed to affect the behavior of the thermal diffusivity in two ways. First, since anharmonic interactions are weaker, there is less phonon-phonon scattering taking place, therefore allowing the extended phonons to make a larger contribution to the thermal diffusivity. Second, the weaker anharmonic interactions means that the contribution to the thermal diffusivity by the localized phonons is reduced since they are more weakly coupled to the extended phonons which serve to facilitate thermally activated hopping of these modes[4]. Why there is weaker anharmonic interactions in the glasses studied here and in [4] than in the glasses studied in [3] is unclear. It may have something to do with the structures of the glasses.

The two-carrier model can also help to explain why the increase concentrations of europium have a stronger effect on the thermal diffusivities at temperatures above room temperatures than at temperatures below. If the two-carrier model is correct in asserting that the density of states of the samples is such that it contains extended phonons, and above a mobility edge, ω_c , localized phonons, then at low temperatures, where the phonons are mostly extended modes, we don't expect for the increases in the density fluctuations introduced by the europium to affect these modes since the extended phonon wavelengths are large enough that they are essentially insensitive to the increase in density fluctuations. On the other hand, at higher temperatures where the extended phonon wavelengths

approach a length scale comparable to the length scale of the disorder in the glasses, the increases in the density fluctuations become more apparent thereby introducing scattering centers which ultimately cause the thermal diffusivity to decrease. The fact that the masses of the europium atoms are much more massive than any of the other elements present in the samples studied here seems to support this.

CHAPTER IV

CONCLUSION

In this experiment the thermal diffusivities of a set of six glasses was studied as a function of temperature. These six glasses differed in the amount of europium concentrations they contained according the compositional formula, $(0.70(\text{SiO}_2)0.03(\text{Al}_2\text{O}_3)0.12(\text{MgO})0.15(\text{Na}_2\text{O}))_{1-x}(\text{Eu}_2\text{O}_3)_x$, where the europium concentration ranged from 0 to 5 molar percent. It was shown that based on the two-carrier model proposed by Dixon and coworkers[3,4], the thermal diffusivity data can be explained fairly well. In this model, the dominant thermal transport mechanism below a mobility edge is through extended state phonons, while above this mobility edge, localized phonons interacting with extended phonons through a three phonon anharmonic process is the main contributor to the thermal diffusivity. The fact that above room temperature, the thermal diffusivity is seen to be linearly dependent on temperature seems to support this. On the other hand, for temperatures below room temperature, if phonon-phonon scattering is assumed to be the main resistive process to the thermal transport by extended phonons, a thermal diffusivity that is a decreasing function of temperature suffices to describe the data well. Furthermore, the fact that as the concentration of europium increases, the thermal diffusivities decrease supports the existence of a phonon spectrum that contains both extended phonons and, above a mobility edge, ω_c , localized phonons.

In this analysis the mobility edge and the frequencies of the localized phonon modes were obtained from Raman data which together with a Debye and Einstein approximation were used to calculate the total heat capacity and the heat capacity of the extended phonons.

REFERENCES

- [1] *The Physics of Amorphous Solids* by Zallen, Richard (John Wiley & Sons, Inc., US 1983).
- [2] *Effects of Modes of Formation on the Structure of Glasses*, edited by R. A. Weeks and D. L. Kinser, pp. 21-30 (Trans Tech Publications Ltd, Switzerland 1987).
- [3] B. D. Gault, G. S. Dixon, J. P. Wicksted, P. A. Watson, and Shu-yun Shi, *Phys. Rev. B* **49**, 257 (1994).
- [4] W. P. Allen, L. Devlin, T. Doyle, R. Snider, P. A. Watson, and G. S. Dixon, *Phys. Rev. B* **49**, 265 (1994).
- [5] *Defects and Disorder in Crystalline and Amorphous Solids*, edited by C. R. A. Catlow (Kluwer Academic Publishers, Netherlands 1994).
- [6] *Effects of Modes of Formation on the Structure of Glasses*, edited by R. A. Weeks and D. L. Kinser, pp. 305-414 (Trans Tech Publications Ltd, Switzerland 1987).
- [7] W. H. Zachariasen, *J. Am. Chem. Soc.*, **54**, 3841 (1932)
- [8] B. E. Warren, H. Krutter, O. Morningstar, *J. Am. Ceram. Soc.*, **19**, 202 (1936)
- [9] R. Orbach, *J. Non-Cryst. Sol.* **164**, 917 (1993).
- [10] B. Golding, J. E. Graebner, and L. C. Allen, *Phys. Rev. B* **34**, 5696 (1986).
- [11] S. Alexander, O. Entin-Wohlman, and R. Orbach, *Phys. Rev. B* **34** 2726 (1986).
- [12] A. Jagannathan, R. O. Orbach, and O. Entin-Wohlman, *Phys. Rev. B* **39**, 13465 (1989).
- [13] *Amorphous Solids*, edited by W. A. Phillips (Springer-Verlag, Berlin, 1981).
- [14] R. C. Zeller and R. O. Pohl, *Phys. Rev. B* **4**, 2029 (1971).
- [15] D. Walton, *Solid State Commun.* **14**, 335 (1974).
- [16] S. Alexander, C. Laermans, R. Orbach, and H. M. Rosenberg, *Phys. Rev. B* **28**, 4865 (1983).

VITA

Candidate for the Degree of
Master of Science

Thesis: THERMAL DIFFUSIVITY IN Eu^{3+} DOPED GLASSES

Major field: Physics

Biographical:

Personal Data: Born in New York City, New York, on June 21, 1969.

Education: Graduated from John F. Kennedy High School, Bronx, New York, in June 1987. Received the Bachelor of Science degree in Physics from the State University of New York College at Cortland in December, 1991. Completed the requirements for the Master of Science in Physics from Oklahoma State University in December, 1995.

Professional Experience: Graduate Teaching Assistant, Oklahoma State University, August 1992 to May 1994. Graduate Research Assistant, Oklahoma State University, May 1994 to present. Research Assistant, Argonne National Laboratory, January 1992 to May 1992. Research Assistant, Temple University, June 1990 to August 1990. Laboratory Technician, Cortland State College, January 1988 to December 1991.